Willans Line Modeling for Powertrain Analysis and Energy Consumption of Electric Vehicles

Dan Raymond Harvey

Thesis submitted to the faculty of the Virginia Polytechnic Institute and State University in partial fulfillment of the requirements for the degree of

Master of Science

In

Mechanical Engineering

Douglas J. Nelson, Chair
Scott T. Huxtable
Michael W. Ellis

June 2nd, 2021
Blacksburg, VA

Keywords: Electric vehicles, vehicle modeling, vehicle efficiency, electric vehicle energy consumption.

Willans Line Modeling for Powertrain Analysis and Energy Consumption of Electric Vehicles

Dan Raymond Harvey

ABSTRACT

With electric vehicles becoming increasingly prevalent in the automotive market consumers are becoming more conscientious of total driving range. In light of this trend, reliable and accurate modeling methods are necessary to aid the development of more energy efficient vehicles with greater drivable range. Many methods exist for evaluating energy consumption of current and future vehicle designs over the US certification drive cycles. This work focuses on utilizing the well-established Willans line approximation and proposes a simplified modeling method to determine electric vehicle energy consumption and powertrain efficiency. First, a backwards physics-based model is applied to determine tractive effort at the wheel to meet US certification drive cycle demand. Second, the Willans line approximation then augments the tractive effort model and parameterizes the vehicle powertrain to establish a bi-directional power flow method. This bi-directional approach separates propel and brake phases of the vehicle over the certification City and Highway drive cycles to successfully isolate the vehicle powertrain from non-intrinsic losses, such as parasitic accessory loads. The proposed method of bi-directional modeling and parameter tuning provides significant insight to the efficiency, losses, and energy consumption of a modeled electric vehicle strictly using publicly available test data. Results are presented for eight electric vehicles with production years varying from 2016 to 2021. These electric vehicles are chosen to encapsulate the electric vehicle market as performance electric vehicles to smaller commuter electric vehicles are selected. All

vehicles are modeled with an accessory load constrained between 300 and 850 W and a regenerative braking ("regen") low-speed cutoff of 5 mph with six of the eight vehicles modeled with a regenerative braking fraction of 94%. The bi-directional Willans line is then tuned to reach agreement with the net EPA energy consumption test data for each vehicle with the results presented as representative of the chosen vehicle. Lastly, a transfer function relating major model inputs to the output is derived and lends considerable insight for the sensitivity of the modeling method. Sensitivity of the proposed modeling method is conducted for a 2017 BMW i3 with the model deemed reasonably resilient to changes in input parameters. The model is most sensitive to changes in powertrain marginal efficiency with a 6% decrease of marginal efficiency leading to a 0.404 kW and 0.793 kW cycle average net battery power increase for the City and Highway drive cycles respectively. Additionally, the model is also sensitive to changes in vehicle accessory load with a direct relationship between increases of vehicle accessory load to increases of cycle average net battery power for the City and Highway cycles. The sensitivity results justify the use of the proposed model as a method for evaluating vehicle energy consumption and powertrain efficiency solely using publicly available test data.

Willans Line Modeling for Powertrain Analysis and Energy Consumption of Electric Vehicles

Dan Raymond Harvey

GENERAL AUDIENCE ABSTRACT

Developing robust and accurate methods for analyzing electric vehicle energy consumption and powertrain efficiency is of great interest. For the purposes of this paper, powertrain refers to a motor / inverter pair which is coupled to a simple gear reduction for torque multiplication. Many vehicles are designed with motors of varying power and torque capabilities which can present challenges when attempting to effectively compare electric vehicles from different manufacturers. The proposed modeling method presented in this work utilizes public test data to derive detailed vehicle and powertrain information. Vehicle energy consumption is also modeled and compared to net EPA test data. Eight electric vehicles are modeled with each vehicle representing a specific segment of the current electric vehicle market. A bi-directional Willans line is applied to model the propel and brake phases of each electric vehicle over the US certification drive cycles. The bi-directional approach effectively isolates the vehicle powertrain from non-intrinsic losses. From the derived powertrain parameters and modeled energy consumption, the proposed method is deemed accurate and highly useful for translating public test data to detailed vehicle information. Lastly, a sensitivity analysis is presented with the proposed method deemed reasonably resilient to changes in input parameters. The modeling method is most sensitive to changes of powertrain marginal efficiency and vehicle accessory load but constraining these inputs to reasonable ranges for electric vehicles proves sufficient.

Acknowledgments

I would like to thank and acknowledge my loving and supportive family who have immensely assisted me throughout my entire college career.

I also would like to thank all of the friends and colleagues I had the pleasure of working with and getting to know over my 6 years at Virginia Tech. There were many times when work became hectic and stressful, but we always guided and supported one another and for that I will always be grateful.

To my committee: thank you Dr. Huxtable and Dr. Ellis for your continued support and guidance.

Finally, I would like to express my sincerest gratitude to Dr. Nelson and all of HEVT who helped make the almost 4 years on the team an unforgettable experience. To Dr. Nelson, I cannot express how grateful I am to have been a part of such a team, and for having the opportunity to work under such an experienced and knowledgeable mentor. Your patience, guidance, and feedback has helped me become the engineer I am today.

Contents

List of Figures

List of Tables

List of Symbols

F_{aero}	Aerodynamic force
F_{roll}	Rolling resistance force
F_i	Inertia force
F_{grade}	Grade force
F_{RL}	Road load force
F_{TR}	Tractive force
A, B, C	Road load coefficients
V_{avg}	Average velocity
a	Acceleration
f_i	Inertia factor
m	Mass
RF	Regen fraction
P_{TR}	Tractive power
P_{TR}^{+}	Propel tractive power
P_{TR}^{-}	Brake tractive power
P_{TR}^{net}	Net tractive power
P_{Regen}	Regen braking power
$P_{Regen,max}$	Max regen power
P_{Fric}	Braking power
P_{mot}^{+}	Propel motor power
P_{mot}^{-}	Regen motor power
P_{bat}^{+}	Propel battery power
P_{bat}^{-}	Regen battery power
P_{bat}^{idle}	Idle battery power
P_{bat}^{net}	Net battery power
P_{accy}	Accessory load
$P_{loss,PT}$	Powertrain loss power (offset)
$P_{bat,DC}^{cyc}$	Drive cycle net battery power
$EVSE$	Electric Vehicle Supply Equipment

E_{TR}	Tractive energy (general)
E_{TR}^{+}	Propel tractive energy
E_{TR}^{-}	Brake tractive energy
E_{TR}^{net}	Net tractive energy
E_{mot}	Motor energy
E_{accy}	Accessory energy
$E_{loss,PT}$	Powertrain loss energy
E_{max}	Battery system max energy
E_{use}	Battery system usable energy
E_{grid}	AC grid energy
E_{chrg}	Offboard charger output energy
E_{rechrg}	Battery system recharge energy
$E_{loss,chrg}$	Offboard charger energy loss
$E_{loss,rechrg}$	Onboard vehicle charger energy loss
$E_{bat}^{+/-}$	Propel or regen battery energy
E_{bat}^{idle}	Idle battery energy
E_{bat}^{net}	Net battery energy
$E_{prim,AC}^{cyc}$	Cycle AC battery energy consumption
$E_{bat,DC}^{cyc}$	Cycle DC battery energy consumption
FE	Fuel economy
η_{chrg}	Charging efficiency
$marg\ eff$	Marginal efficiency
$slope^{+}$	Propel slope
$slope^{-}$	Brake slope
$offset$	Powertrain offset
ME_{net}	Net powertrain marginal efficiency
$Offset_{net}$	Net powertrain offset
d_{cyc}	Cycle distance
t_{cyc}	Cycle time

Chapter 1
Introduction

Vehicle modeling is a highly motivated area of interest for estimating vehicle energy consumption, determining acceleration performance, optimizing designs, and selecting components. The power of analytically evaluating a vehicle lies in the elimination for the need of detailed test data. Willans line modeling is a well-established method for applying a linear approximation to evaluate system power requirements and power output capabilities. A Willans line model is a transfer function relating input power to output power through a linear equation constrained by a slope and an intercept, here referred to as the offset. A general example of a Willans line model is illustrated in Figure 1.1 with the slope and offset labelled. The slope and offset are considered model inputs and represent the behavior of the modeled system. The slope of the Willans line determines the necessary input power to meet a desired output power, and the offset reflects the system power loss. The inverse of the Willans line slope is referred to as the marginal efficiency of the system. The marginal efficiency is related to the efficiency of the system but the two must be distinguished from one another. The marginal efficiency cannot exceed unity and represents the efficiency limit of the system. If the marginal efficiency exceeds unity the required input power would decrease as the desired output power increases, violating the laws of thermodynamics. In reference to Figure 1.1, the offset of the Willans line is set to 1 kW with a slope of 2.5 which correlates to a marginal efficiency of 40%. Deriving the efficiency is possible by using the Willans line slope and offset. Figure 1.2 represents the same system presented in Figure 1.1 with an efficiency curve plotted. With input and output power established from the slope and offset, the efficiency can be calculated by taking the ratio of output to input power. An

asymptotic efficiency relationship is derived from the Willans line slope and offset shown in Figure 1.2 with the efficiency limit eventually reaching the marginal efficiency of 40%. Willans line models provide a method for modeling the power requirements of a system and for establishing the operating efficiency. Willans line models can be applied to internal combustion engines for relating the fuel input power for producing a desired engine output power. Willans line models are also applied for quantifying vehicle energy consumption over speed versus time drive cycles.

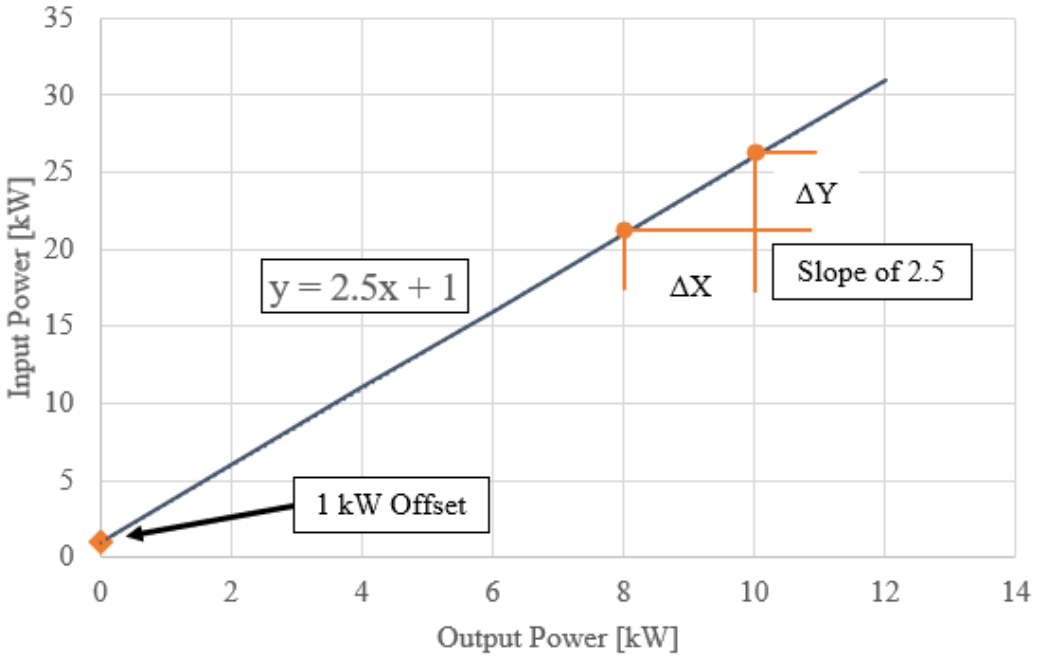

Figure 1.1: *Willans Line with Labelled Slope and Offset*

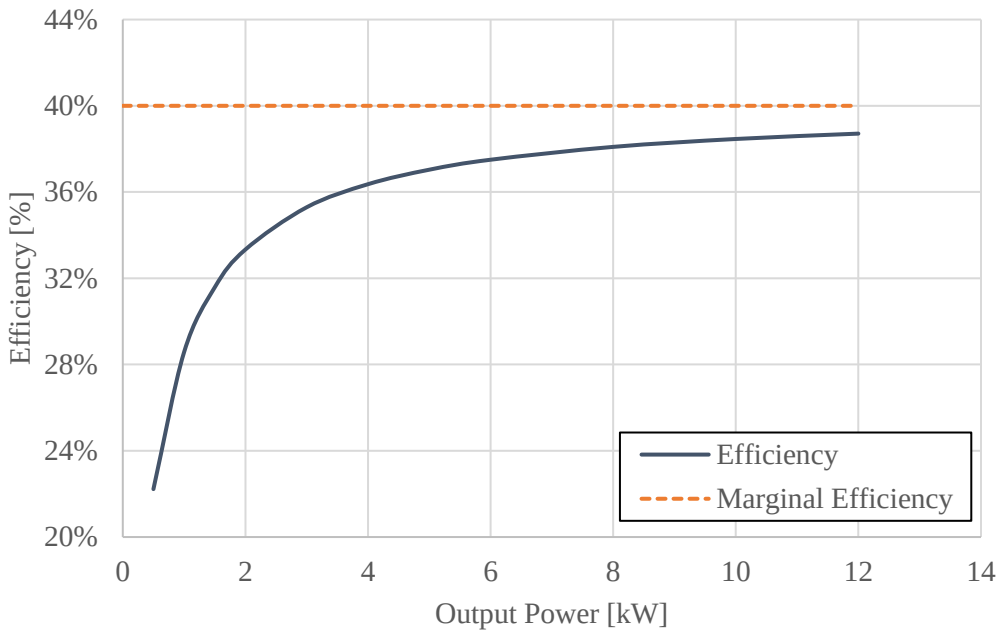

Figure 1.2: *Efficiency Curve Derived from Willans Line Slope and Offset*

The work presented here applies the Willans line approximation extended to electric vehicles which intrinsically have bi-directional power flow. Electric energy is discharged from an energy storage system to propel the vehicle, and braking energy can be recaptured by the electric motor system for storage. As such, developing a bi-directional Willans line which encapsulates this bi-directional power flow for electric vehicles can be greatly useful. Due to the bi-directional power flow of electric vehicles, the efficiency of the system can get clouded by vehicle accessory load, regenerative braking fraction, and other non-powertrain related losses. Therefore, the work presented here proposes a bi-directional Willans line to characterize the powertrain of electric vehicles more effectively while simultaneously evaluating vehicle energy consumption over US certification drive cycles. The bi-directional Willans line model is developed and applied using public test data available from the EPA. To this end the major objectives of this work are to first develop a bi-directional power flow Willans line model which appropriately partitions the propel and brake phases of the vehicle. Second, to establish a method for evaluating vehicle net energy

consumption over certification drive cycles. Third, to lend insight to the vehicle powertrain parameters such as power loss and system efficiency. Lastly, to achieve the previous three objectives by only using publicly available test data reported by EPA. The last objective is significant because detailed vehicle information is not needed with the proposed method which greatly simplifies data collection. The sensitivity of the proposed method is additionally explored to determine the resiliency of the method to changes of input parameters.

Chapter 2
Literature Review

Previous work in conventional and electric vehicle modeling is well-established and discussed abundantly in literature. The motivation for evaluating vehicle energy consumption is deeply rooted within both industry and government. The bi-directional Willans line utilizes some similar methods proposed previously in the literature reviewed here. Indeed, the Willans line method is well-established for conventional vehicles, but there is a lack of work with applying the Willans line method to electric vehicles. This work applies Willans line modeling to develop a simplified, yet accurate, method for evaluating electric vehicle energy consumption. Additionally, the bi-directional Willans line is derived purely from publicly available data and creates an adaptable vehicle model. The previous work discussed in this section is focused on other vehicle modeling methods, linear approximations for powertrain modeling, and determining vehicle energy consumption over US drive cycles. Similar methods which are applied in the bi-directional Willans line are identified in addition to the novelty of the method overall.

The work performed in [1] consists of aggregating vehicle parameters and data of the most marketed electric vehicles of 2014 and 2015. The analysis is motivated by a need to compile electric vehicle data and to draw comparisons across different makes and models. Because others can build off the data collected, the work conducted in [1] assists future efforts in vehicle modeling. The authors elect to separate propel and brake phases of each vehicle to determine discharge and recharge energy, similar to what is proposed in this work. The method determines battery discharge and recharge energy which requires detailed component information that is unfortunately rarely reported by manufacturers. General trends are formed around vehicle frontal

area and drag coefficients for determining aerodynamic effects and estimating vehicle rolling resistance. However, information for estimating frontal area and the drag coefficient is typically rarely available to the public. The work proposed here utilizes ABC coefficients published by EPA to generalize the road load force which eliminates the need for detailed vehicle data.

The model developed in [2] analyzes the use of a PID driver model to determine commanded vehicle acceleration to meet the City and Highway drive cycle demands. Driver models are well-established and researched, and the authors elect to use the Ziegler-Nichols method for tuning and optimizing the driver model. Ultimately, the vehicle and driver model are validated against published Nissan Leaf data which follows similar trends performed in this work. The results illustrate both the capability and utility of validating a model using EPA energy consumption data. Due to a lack of regenerative braking information for the modeled vehicle, the authors make estimations and then prove the model is reasonably insensitive to changes in regen braking parameters. The results presented illustrate the accuracy of validating a model to EPA data and how parameter estimation in the absence of vehicle data can still yield effective results.

The methods applied in [3] somewhat mirror that of [1][2] in which a physics based approach is used for determining vehicle energy consumption. The work performed is centered around conventional vehicles with select hybrids additionally included. No inertia effects are considered within [3]. This work adds a correction factor to the linear inertia of the vehicle that encapsulates the rotating inertia effects of the vehicle tires when accelerating and decelerating. The primary goal of [3] is to identify the fuel economy improvements enabled by new powertrain technology in comparison to older powertrain architectures. As such, older model year vehicles are compared against newer model year vehicles to draw trends on multi-speed transmissions and other technology improvements. The primary validation method involves comparing modeled

results to available information published by the EPA. Lastly, a second focus of [3] is to provide motivation for continued powertrain technology research to further improve conventional vehicle fuel economy. Therefore, the work is intended strictly for validation versus generating a modeling method which is the primary goal of the work presented in this paper.

There is great industry and government interest for developing accurate, robust, and adaptable modeling methods like the one proposed in [4]. The authors propose the FASTSim model as a tool for determining the impacts of vehicle technology improvements and for comparing powertrains of different vehicles. This model can determine vehicle energy consumption, vehicle efficiency, and battery life for electric vehicles. FASTSim applies 1 Hz drive cycle information to determine various properties of the modeled vehicle with detailed information input. Major inputs to the model in [4] are coefficient of drag, frontal area, center of gravity, efficiency curves for electric vehicles, and the vehicle energy management strategy. The latter consists of state of charge limits of the vehicle energy storage system and the logic for how this storage system discharges and recharges energy. Therefore, FASTSim is a reliable and accurate modeling method for analyzing vehicles but requires significant input data that is rarely reported. One of the major focuses of this paper is to utilize public test data for gathering necessary vehicle information; a methodology which allows any user to develop the proposed model.

The model developed in [5] is a continuation of FASTSim with the purpose of identifying eco-routing for vehicles. RouteE is described as a Python package that is trained from FASTSim with over 1 million miles of vehicle data. In addition to the machine learning capabilities of RouteE, vehicle analysis can be performed without the detailed drive cycle or path data. The ability to model a vehicle without detailed drive cycle data is a significant accomplishment as this capability eliminates the need for vehicle dynamometer data. This capability of RouteE was

enabled from the previously mentioned model training, in addition to detailed data of road surfaces. RouteE also allows users to train their own models, which illustrates the adaptability of the developed method. However, to perform unique test cases the user needs physical data and energy consumption metrics to initially train RouteE for the specific use-case; therefore requiring drive cycle or path data. The development of RouteE illustrates the growing capabilities of vehicle modeling overall.

Expanding upon the Willans line method for characterizing and identifying powertrain characteristics and losses is explored in [6]. Conventional vehicles are studied within the work of with the primary goal aimed at correlating Willans line parameters to powertrain losses. The authors also apply the Bishop method for further characterization of the losses generated from the Willans line approximation. The authors also utilize experimental results to draw meaningful trends. Similar to the work proposed here, the authors of [6] apply constant marginal efficiency and power loss terms for constraining the model; a simplification that reduces model complexity yet yields reliable results. From the results, the authors conclude the linear approximation is useful for characterizing powertrain losses and optimizing powertrain design. A simplified model capable of problem optimization further conveys the power and robustness of the Willans line approximation for modeling vehicles.

The application of a power-based Willans line approach is discussed and investigated within the work presented in [7]. Conventional vehicles are studied within the work with goals of determining fuel input power for a given tractive power and characterizing powertrain improvements for increased fuel economy. When developing the power-based approach, the authors of [7] define a cycle average tractive power as being the propel tractive energy divided by the total cycle time. In this work the cycle average tractive power is taken to be the summation of

both propel and brake tractive energies divided by total cycle time. Combining the propel and brake tractive energies is done because of the bi-directional power flow of electric vehicles and to evaluate the net energy consumption reported by EPA to a net tractive effort. The developed power-based approach in [7] is validated against EPA and Argonne National Lab test data that is publicly available. With this data, the authors of [7] conclude the Willans line power-based approach is sufficient at determining the corresponding fuel input power to propel the vehicle over varying drive cycles. With model validation established, the analysis then shifts to studying the effects of road grade and increased accessory load (e.g. operating the air conditioning compressor). The model is then run for varying road grade to determine the input fuel power with reasonable results obtained. Slight deviation is shown at higher vehicle speeds, but accurate results are generated for lower vehicle speeds. Second, when accessory load is increased a direct correlation between model offset is observed which illustrates the impact an increased accessory load has on energy consumption and power demand. Lastly, several normalization methods are proposed within [7] for comparing vehicles with differing mass, engine displacement, and performance metrics. The results convey the power and utility of a linear approximation for estimating vehicle energy consumption, as well as for modeling vehicle powertrains. Vehicles with different powertrains are condensed onto a single transfer function when the cycle average fuel and tractive power are both normalized by vehicle mass. This method of normalization is shown to be useful for comparing vehicles with similar performance but different mass. For comparing vehicles of differing performance, the authors propose a normalization method of rated power to vehicle mass. These two normalization methods show great utility for condensing different vehicles onto a single transfer function for effective comparison. The work performed in [7] shows great potential in the realm of applying linear approximations to model vehicle powertrains and energy consumption.

Chapter 3

Model Background

Tractive Effort Model Development

Before the bi-directional Willans line can be applied, a tractive effort model is developed from 1 Hz dynamometer data available through EPA [8][9]. This section discusses how the tractive effort portion of the model is developed and all governing equations. Figure 3.1 depicts the forces acting on a vehicle when driving on a road surface with propelling the vehicle being taken as positive, and braking considered negative. There are four major forces which act on a vehicle: the aerodynamic force (F_{aero}), the rolling resistance force (F_{roll}), the inertia force (F_i) and the grade force (F_{grade}). The aerodynamic force is proportional to the vehicle speed and increases quadratically as speed increases; this force dominates at higher speeds and is typically the limiting factor for vehicle top speed. The rolling resistance force is related to tire dynamics and how the contact patch is formed on the road surface; this force has both a static and speed dependent portion. The inertia force is present whenever the vehicle is accelerating or decelerating and includes rotating inertia effects from the vehicle tires; this force typically dominates at lower speeds when the vehicle is accelerating from a stop. Lastly, the grade force is not always present but is equivalent to the force acting on the vehicle when moving up or down a slope. This force acts against vehicle motion when moving uphill and acts along vehicle motion when moving downhill. This force can be significant and can drastically increase vehicle energy consumption. US certification drive cycles do not contain any road grade. Road grade is not considered in this work, but the model can easily account for a known road grade as an input.

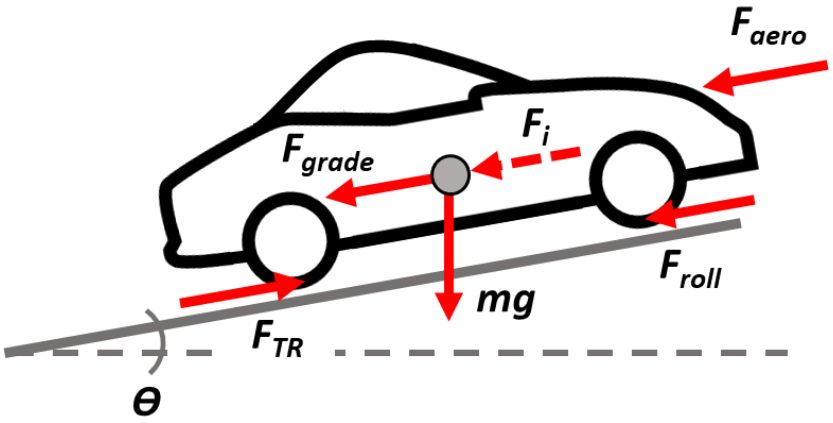

Figure 3.1: *Forces Acting on a Vehicle When Driving*

The road load force is the summation of all forces acting on the vehicle when in motion and can be explicitly written as

$$F_{RL} = F_{grade} + F_{roll} + F_{aero} \tag{3.1}$$

with the tractive force being the summation of all forces acting on the vehicle when propelling or braking and is written explicitly as

$$F_{TR} = F_{RL} + F_i \tag{3.2}$$

with F_i being the only additional force considered. ABC coefficients, also referred to as road load parameters, are taken from published EPA data in the Test Car List and Application for Certification reports [8][10]. These road load parameters are given for all vehicles sold in the US. Therefore, road load force F_{RL} without considering road grade is directly calculated from the following equation

$$F_{RL} = A + B \cdot V + C \cdot V^2 \tag{3.3}$$

where A is most related to the static rolling resistance coefficient from the vehicle tires contacting the road surface. B is most correlated to a speed dependent rolling resistance term which encapsulates physical changes to the tire contact patch on the road surface as vehicle speed changes. C is most related to the aerodynamic force acting on the vehicle as this term is multiplied

by speed squared. By utilizing the ABC coefficients, the vehicle road load force F_{RL} is calculated for the City and Highway certification drive cycles. EPA reports fuel economy data for all vehicles for both City and Highway certification drive cycles. This data allows for model validation for each vehicle for the City and Highway cycles. To give additional detail, the City certification drive cycle is commonly referred to as the Urban Dynamometer Driving Schedule (UDDS) and the Highway certification drive cycle is referred to as the Highway Fuel Economy Test (HWFET). Both drive cycles are considered 'mild' which refers to the drive cycle speed, acceleration, and power demand. Table 3.1 includes speed and acceleration characteristics of each drive cycle. As is expected, the average speed of the UDDS is representative of city driving while the HWFET average speed is representative of highway driving. The UDDS consists of frequent stops with idle times whereas the HWFET consist of only one stop which is at the end of the cycle.

Table 3.1: *Certification Drive Cycles Speeds and Accelerations*

Drive Cycle	Average Speed	Maximum Speed	Peak Acceleration
	[mph]	[mph]	[m / s^2]
City (UDDS)	19.5	56.7	1.48
Highway (HWFET)	48.3	59.9	1.43

Over each of these drive cycles there is a varying speed profile which each tested vehicle must follow. These two certification cycles are used to standardize testing and to fairly measure energy consumption of vehicles. In addition to the varying speed profiles there are three key vehicle operational states over each cycle: propel, brake and idle. Propel is the phase during which a positive tractive force is required at the wheels while braking is when the tractive force is negative. Propel and brake are identified within the model per the tractive force. A positive tractive force correlates to propel and a negative force correlates to brake. Idle is the phase when the vehicle is completely at rest and is neither accelerated nor moving. During the idle phases, no energy is consumed to drive the vehicle and the vehicle accessory load is the only power requirement the

vehicle must meet. The accessory load is the power required to operate lights, powertrain cooling, and electronic systems separate from the powertrain itself. Additional accessory loads due to cabin heating and cooling can be included but are not part of the drive cycle data used for model validation.

With the operational states well defined, the speed requirements of each drive cycle are then used to develop a "backward" model which determines total tractive effort at the wheel for propelling and braking the vehicle and thus powertrain demand. A "backward" model considers the output known and calculates "backwards" the corresponding input. In the case of the model proposed here, the drive cycle speed is considered the output and the battery discharge or recharge energy is considered the input. Each drive cycle is discretized into 1 Hz steps where each time step represents the instantaneous vehicle speed. The vehicle speed is then integrated over each time step to determine the average travelling speed when going from t_{n-1} to t_n from the following equation

$$V_{avg}(t_n) = \frac{V(t_n) + V(t_{n-1})}{2} \tag{3.4}$$

where V_{avg} is the integrated vehicle speed at time t_n and is taken to be representative of the travelled speed when moving between two time steps. The vehicle acceleration at time step t_n is then calculated by differentiating the instantaneous velocity between time steps t_{n-1} and t_n

$$a(t_n) = \frac{V(t_n) - V(t_{n-1})}{t_n - t_{n-1}} \tag{3.5}$$

where a is the vehicle acceleration in m/s^2 at time. EPA provides drive cycle information in 1 Hz time steps which enables vehicle acceleration in Equation 3.5 to be determined by simply taking the difference of instantaneous vehicle velocity. With vehicle acceleration known, the inertia force is then be found from the governing equation

$$F_i = m \cdot f_i \cdot a \tag{3.6}$$

where m is the test mass of the modeled vehicle as stated by EPA, f_i is a scalar multiple related to rotating inertia effects and a is the previously determined vehicle acceleration. The inertia factor f_i has been well explored and documented in literature, as discussed in [11] where a factor of 1.03 is used. A factor of 1.04 is applied here to represent larger wheels and tires on modern vehicles when compared to the vehicles studied in [11]. From here, with average vehicle velocity and acceleration determined, the tractive force required to propel and brake the vehicle is calculated using Equation 3.2. Lastly, the tractive power for propelling and braking the vehicle is determined from the following

$$P_{TR} = F_{TR} \cdot V_{avg} \tag{3.7}$$

where P_{TR} takes positive or negative values depending on the operating state of the vehicle. If P_{TR} is negative the vehicle is braking, denoted by P_{TR}^-, and if P_{TR} takes positive values the vehicle is propelling, denoted by P_{TR}^+. This tractive power is representative of what the vehicle must ultimately produce at the wheel to travel the specified drive cycle speed. The propel and brake tractive powers P_{TR}^+ and P_{TR}^- are found on a second by second basis because 1 Hz drive cycle data is used. Performing these calculations for each time step allows for the vehicle power to be determined discretely, which leads to the tractive energy at the end of the drive cycle being equivalent to the following

$$E_{TR} = \sum P_{TR} \cdot \Delta t \tag{3.8}$$

where E_{TR} is the tractive energy requirement at the wheel over the entire drive cycle. Using 1 Hz drive cycle data enables E_{TR} to be directly found without needing to consider the time difference as the tractive power P_{TR} is determined on a second by second basis. Separating the tractive power into propel and brake phases enables the corresponding propel and brake tractive energy to be

determined. E_{TR}^{+} and E_{TR}^{-} reflect two separate operational states which must be combined to yield a net cycle energy. Therefore, the net tractive energy can be directly determined from Equation 3.8 by summing all power quantities over a drive cycle, or from performing the following

$$E_{TR}^{net} = E_{TR}^{+} + E_{TR}^{-} \tag{3.9}$$

where E_{TR}^{net} is the net energy value over the drive cycle. By calculating E_{TR}^{net} the tractive effort portion of the model is established and the bi-directional Willans line can be built in.

Vehicle Powertrain Model Development

Building onto the tractive effort model to include vehicle powertrain characteristics with data available through EPA allows the power flow from battery to wheel to be determined. The vehicle parameters necessary to determine tractive effort are the road load coefficients and vehicle test mass; no powertrain data, fuel economy information or energy consumption are required. Additional information from the Application for Certification data is gathered for modeling the vehicle powertrain. The additional data includes battery energy capacity, the AC recharge event energy consumption, the vehicle range, and the reported fuel economy for the City and Highway cycles. Accessible and publicly reported data are the only inputs for the model proposed in this work; a major advantage as data collection is simplified and model complexity is reduced. This section focuses on how the electric vehicle model is developed and the necessary vehicle data used. A brief introduction to electric vehicle operation is also provided which lends insight to how the bi-directional linear approximation is applied.

The power flow of an electric vehicle during propel and brake phases needs to be understood before the governing equations are introduced. Figures 3.2 – 3.5 illustrate the power flow from battery to wheel for propel events, wheel to battery for brake events, the end of drive

cycle phase, and the recharging event of the vehicle. Electric motors can operate in a discharge (propel) phase and recharge (braking) phase, with the latter allowing energy to be recuperated by the high-voltage battery system. The braking operational phase is a key difference from conventional vehicles as gasoline fueled engines cannot recapture brake energy. Shown in Figures 3.2 – 3.4 is the vehicle powertrain modeled as coupled unit. This approach is used as modeling the powertrain as one unit eliminates the need for separately estimating motor and gearbox efficiencies. This approach then leads to all derived parameters being indicative of the powertrain as an entire unit. Referring to Figure 3.2, propelling the vehicle requires power to be drawn from the battery to power the electric traction motor. The electric traction motor then supplies the necessary power to the wheels for meeting the speed and acceleration requirements. In Figures 3.2 – 3.4 losses are illustrated when going from battery to wheel. These losses decrease the total amount of delivered power. Delivered power refers to the power output at the wheels for propel and the regenerative power at the battery during braking. Figures 3.2 & 3.3 also depict the vehicle accessory load as taken directly off the high-voltage bus; therefore, the delivered power is subsequently decreased proportionally with the accessory load of the vehicle. The accessory load is taken to always be on and constant. Every vehicle has a different accessory load, but for purposes of this work the accessory load is taken to be within the range of 300 – 850 W for all modeled vehicles; a simplification that is explained in the Results and Discussion section. Another note to make is during braking events the definition of input and output power is reversed due to the power flow direction switching. Figure 3.3 illustrates the braking power at the wheel which is fed back into the motor system. As will be explained later, the proportion of the braking power which is diverted to the motor system is defined as the regen fraction *RF*. The regen fraction is a constant percentage of the total braking power that is sent back to the motor for recapture. To

maintain stability and handling of the vehicle the remaining braking power is sent to traditional brakes. Details of the regenerative braking logic in this work are discussed in the Results and Discussion. Since the direction of power flow switches during braking, the braking power sent back to the traction motor represents the maximum available power for recapture. Therefore, the delivered power to the battery terminals will always be less than the braking tractive effort and the regen braking power due to losses, limitations, and the accessory load. Referring to Figures 3.4 & 3.5, the end of drive cycle phase is categorized by a discharged battery system which is then recharged to the initial state of charge. During recharge, AC grid energy is supplied to the vehicle onboard charger which converts the AC grid energy to DC energy. While the battery recharges, part of the recharge energy is lost to irreversibilities of the onboard charger, for operating the charger control system, the battery thermal management system, as well as battery charging internal losses . The AC grid energy represents the recharge event energy reported by EPA in AC kWh. Stepping from the AC grid energy reported by EPA to the subsequent battery recharge energy requires insight on a charging efficiency. This charging efficiency is separate from the efficiency of the onboard charger. Making the distinction of AC versus DC energy is key as this work primarily focuses on DC energy consumption of a vehicle to meet drive cycle demand.

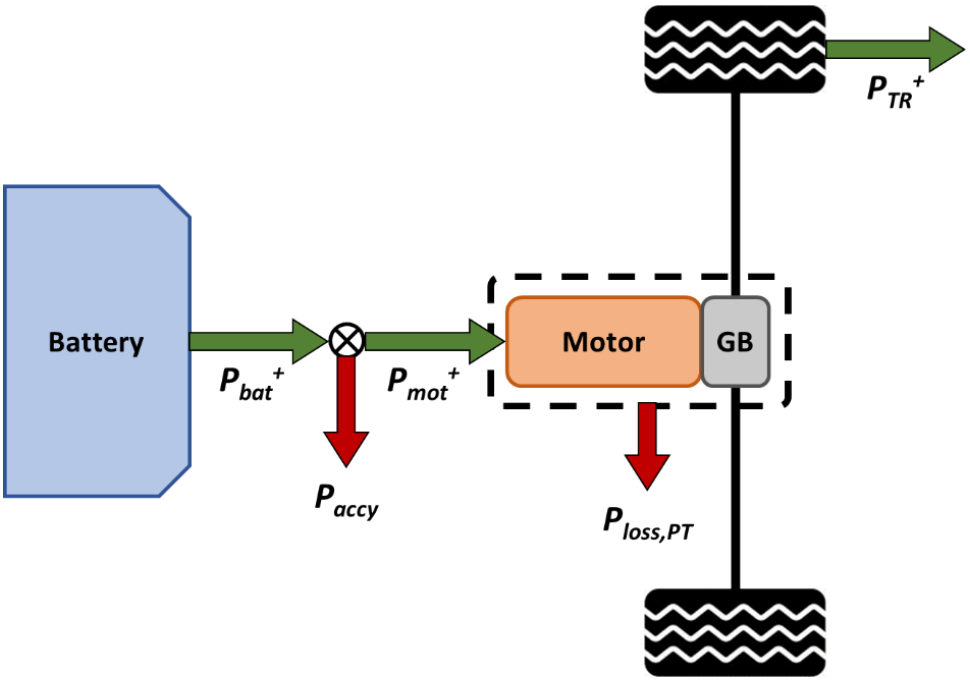

Figure 3.2: *Vehicle Propel Power Flow*

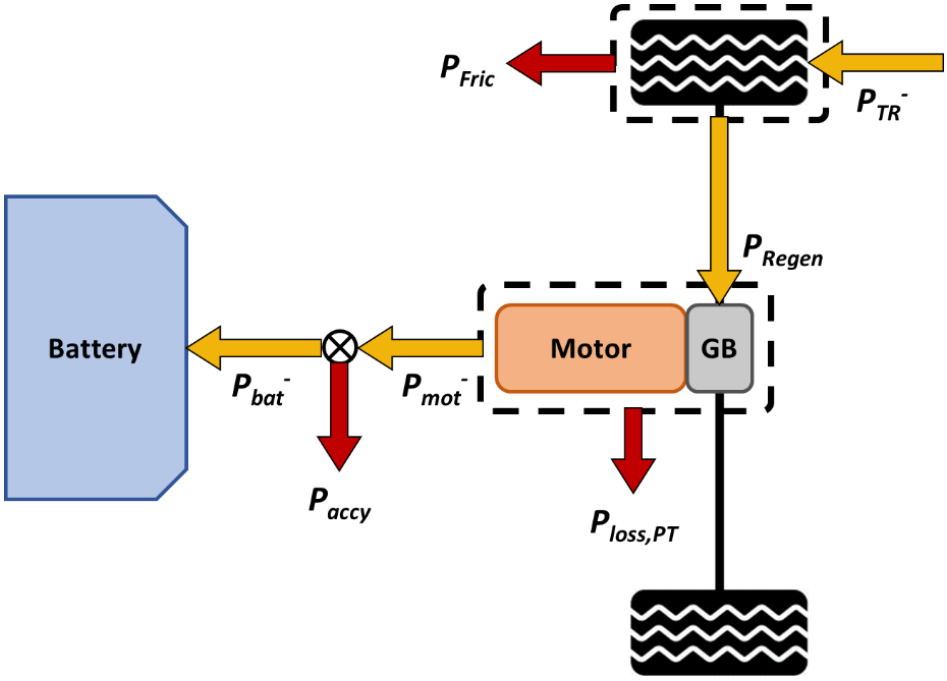

Figure 3.3: *Vehicle Braking Power Flow*

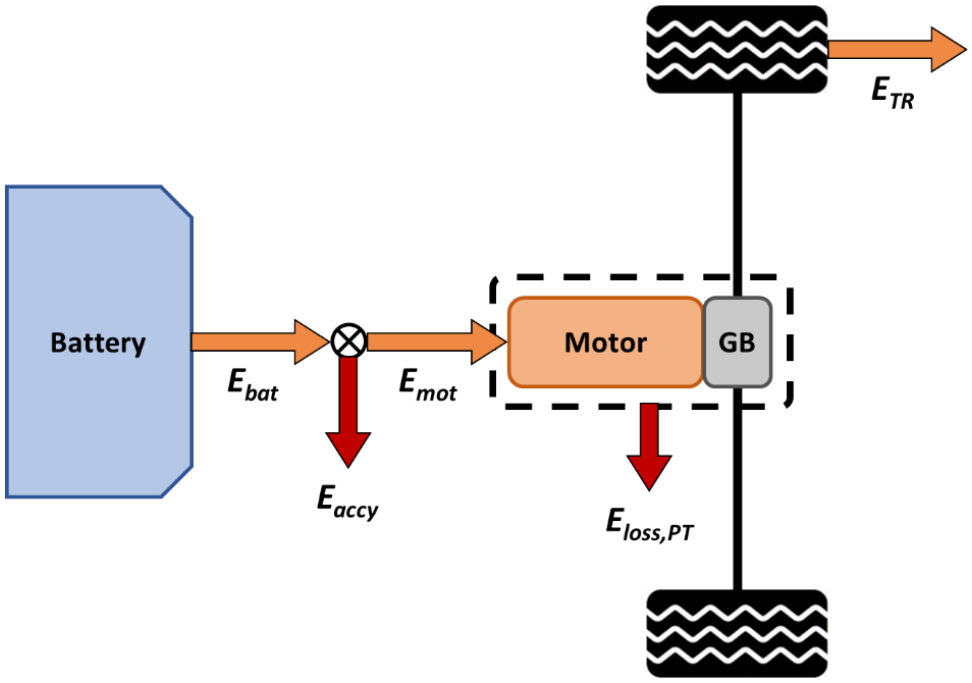

Figure 3.4: *Vehicle Net Energy Flow at End of Drive Cycle*

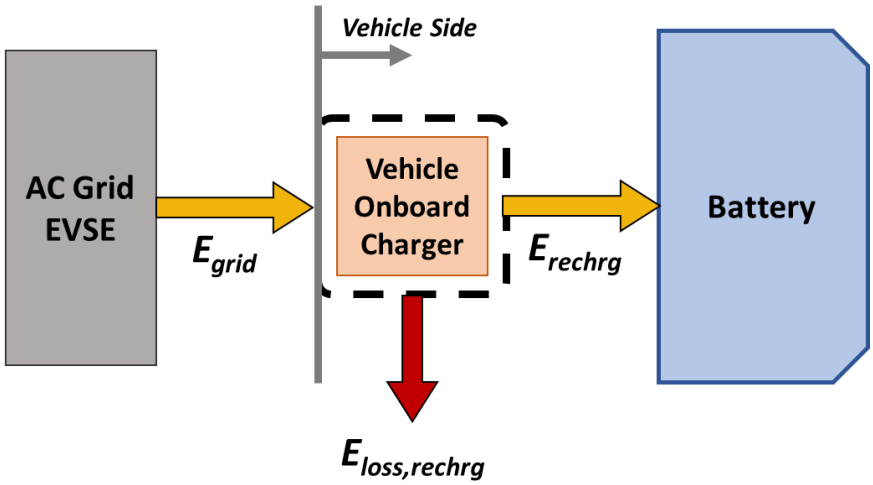

Figure 3.5: *Vehicle Recharge Power Flow*

From the defined power flow definitions, the bi-directional Willans line is then integrated into the 1 Hz tractive effort model. The Willans line method is well-established and utilizes a marginal efficiency and constant offset for relating input power to system output power. The marginal efficiency of a Willans line model is less than unity as input power must be greater than output power. The marginal efficiency in conjunction with the powertrain offset can be used to

model the efficiency of a component. More on using powertrain marginal efficiency and offset to establish efficiency is discussed in the Results and Discussion section. In the bi-directional Willans line model only one marginal efficiency is required as input for modeling propel and brake phases. Due to power flow direction, the slope of the propel Willans line is equal to the inverse of the brake slope. Relating the propel slope to the brake slope is done to capture the expected behavior of a single motor acting as both the motor for propel and the generator for brake. Therefore, the relationship between the input marginal efficiency and propel slope is the following

$$slope^{+} = \frac{1}{marg\ \ eff} \tag{3.10}$$

where $slope^{+}$ will be positive and greater than unity due to $marg\ eff$ being less than unity. During the braking phases of vehicle operation, the input marginal efficiency is directly used to model regenerative braking energy flow. Written explicitly and in same terms as the propel slope, the slope for braking is the following

$$slope^{-} = marg\ \ eff \tag{3.11}$$

where during regenerative braking less power is supplied to the battery than what is available at the wheels. To this end, the propel and braking phases are modeled as distinct phases which comprise the bi-directional nature of the Willans line. With the propel and brake slope defined, the powertrain offset is the final parameter necessary to constrain the model. The powertrain offset is indicative of a power loss which always detracts from the delivered power regardless of propelling or braking the vehicle. Because of this fact and to model the behavior of the vehicle going from propel to brake, the same offset for propel is used for brake. These assumptions for the propel and brake parameters are made to reduce the total number of input parameters for the model and is leveraged by expected motor behavior.

The bi-directional power flow of electric vehicles was previously illustrated and explained in Figures 3.2 & 3.3. Figure 3.2 depicted the propel phase power flow with battery discharge power as the input and tractive effort at the wheel as output. Utilizing a backwards model, the propel slope and Willans line offset are used in conjunction to determine the motor electrical input power for a necessary tractive effort. Therefore, determining the propel motor input power is determined from the following

$$P_{mot}^{+} = P_{TR}^{+} \cdot slope^{+} + offset \tag{3.12}$$

where the propel slope and Willans line offset result in a propel motor input power which is greater than the tractive effort at the wheel. Equation 3.12 models expected behavior. Determining the propel battery discharge power is done by considering the accessory load by the following

$$P_{bat}^{+} = P_{mot}^{+} + P_{accy} \tag{3.13}$$

where the accessory load P_{accy} results in a propel battery discharge power greater than the propel motor input power, which is also to be expected. Equations 3.12 & 3.13 define how the propel Willans line parameters are applied in the bi-directional model for determining propel battery discharge power for known tractive effort. Braking follows similar logic with a few nuances which need defining. Figure 3.3 depicts the braking phase power flow with braking tractive effort as the input and battery recharge power as the output. The change in definition of input and output powers between the propel and brake phases is an important distinction. Whereas during propel phases the discharge battery power is greater than the tractive effort, the battery recharge power during braking will be less than the tractive effort at the wheel. Starting at the braking tractive effort, the proportion which is fed back through the motor system is defined by the following

$$P_{Regen} = RF \cdot P_{TR}^{-} \tag{3.14}$$

where P_{Regen} represents the braking tractive effort reduced by the regen fraction *RF* that is sent back through the motor system for recapture. As is discussed in more detail in the Results and Discussion section, simple logic is found to be sufficient for encapsulating regen brake performance. In addition to the regen fraction, a low-speed cutoff is also enforced which represents the vehicle speed at which regen braking no longer operates. As vehicle speed decreases the availability of energy also decreases, therefore regenerative braking cannot recuperate power at low vehicle speeds. Additionally, to prevent power limits from being exceeded and components becoming damaged, there is a maximum regen brake power that the powertrain can recuperate. Therefore, in high power braking regions the regenerative braking power is limited by a maximum limit and the remaining braking force is handled by friction brakes. The regenerative braking logic in the model consists of the regen fraction *RF*, a low-speed cutoff, and a maximum regen power limit. By using second by second modeling the vehicle speed is continually compared to the cutoff speed to ensure regenerative braking can occur. When the vehicle speed exceeds the cutoff speed, regenerative braking occurs and P_{Regen} is found from Equation 3.14 above for second by second modeling. When the maximum limit is reached, P_{Regen} is set to $P_{Regen,max}$ until P_{Regen} falls eventually below the power limit at a given time interval. This approach is found to be effective when modeling the vehicle over second by second drive cycles to match net EPA energy consumption data. From P_{Regen} the subsequent motor regen power is determined from $slope^-$ and the offset

$$P_{mot}^- = P_{Regen} \cdot slope^- + offset \tag{3.15}$$

where P_{mot}^- is reduced proportionally by the offset and $slope^-$. From the regenerative power feeding back to the battery, the equivalent battery recharge power is found by

$$P_{bat}^- = P_{mot}^- + P_{accy} \tag{3.16}$$

where the accessory load is included. Figure 3.6 depicts how the bi-directional Willans line is applied for propel and brake phases and represents operating points generated by the modeling method and not from EPA test data. The propel and brake operating regions are illustrated on Figure 3.6 with tractive power on the x-axis and battery power on the y-axis. Example propel and brake Willans line curves are also plotted in Figure 3.6. Quadrant 1 represents the propel phases of vehicle operation where $slope^{+}$ and the offset model the required battery power for instantaneous and cycle average propel tractive powers. Quadrant 3 illustrates the regenerative braking region of vehicle operation where $slope^{-}$ and the offset model the battery regenerative power for instantaneous and cycle average regen powers. The propel and brake powertrain parameters are applied in the vehicle model on a second by second basis, which refers to instantaneous tractive powers. However for the purposes of plotting the bi-directional Willans line for the City and Highway cycles, the cycle average propel and regen tractive power is used. Therefore, Figure 3.6 does model the instantaneous power flow of the vehicle, but to represent a drive cycle as a single tractive power point the cycle average tractive powers are used. When tractive effort is 0 kW, the y-intercept is indicative of the constant powertrain system losses (i.e. the powertrain offset), the marginal efficiency includes losses that increase as power increases. An important note to make is the continuity between the propel and brake phases because one offset is defined in the model. Therefore, a vehicle shifting from a propel phase to a braking phase will transition from the propel Willans line to the brake Willans line. Although the propel and brake curves are continuous at the y-intercept, the slope of each curve changes because of the change in the definition of input and output power. During propel the tractive effort is the output whereas during braking the tractive effort is the input. Referring to Figure 3.6, when the motor regenerative power is 0 kW the x-intercept represents the regen power necessary for overcoming

system losses. In other words, a regen power that is greater in the negative direction than the x-intercept will result in power being recuperated by the high-voltage battery system. Plotting battery power against instantaneous tractive / regen power is done as a method for further isolating the powertrain non-intrinsic losses. Because a bi-directional Willans line is created to model propel events separate from braking events, four operating points are shown in Figure 3.6. By modeling the propel power flow separate from the braking power flow the battery power for corresponding propel and brake tractive powers is determined. The bi-directional method generates a propel operating point for the City and Highway drive cycles and a braking operating point for the two drive cycles. This results in a total of four modeled operating points as shown in Figure 3.6. Therefore, Figure 3.6 illustrates the bi-directional Willans line method for modeling propel and brake battery powers for instantaneous tractive powers. Combining the modeled propel, brake, and idle battery powers yields a net power value which is tuned by the input parameters to match EPA net energy consumption data. Net power plots are presented in this work and illustrate the power discharge from the battery to meet accessory load, component losses, and tractive effort which makes isolating the powertrain more difficult. The ability to isolate the vehicle powertrain from accessory load and other non-powertrain intrinsic losses is a major proponent of the modeling method. Isolating the powertrain in this fashion allows for easier cross-comparison of vehicle makes and models. The distinction of the bi-directional Willans line is extremely important because separating propel and brake phases of vehicle operation by using two separate but related curves is the novel approach suggested in this work.

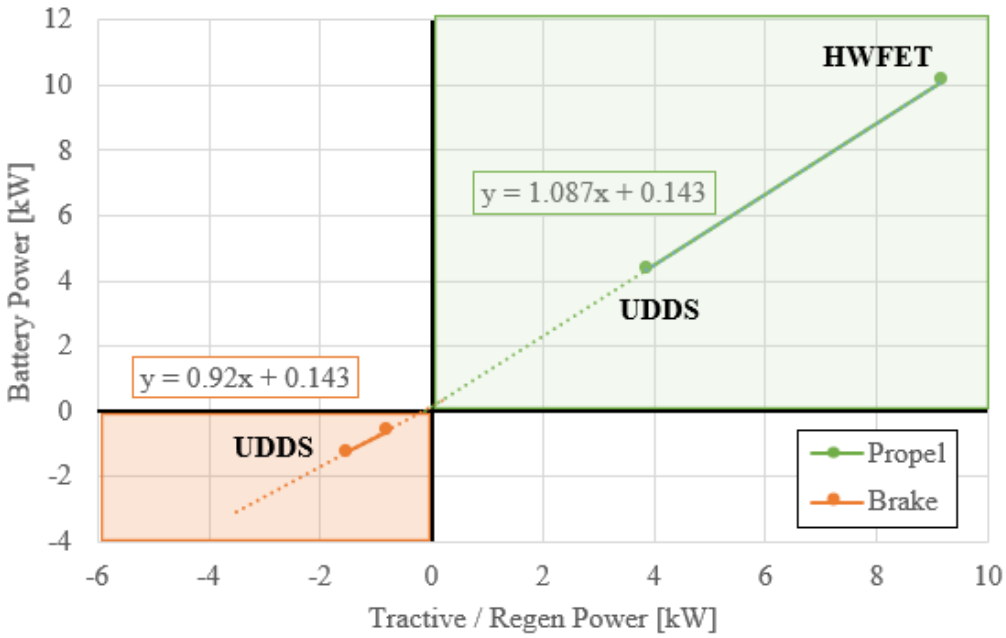

Figure 3.6: *Instantaneous Battery Power for Propel and Brake Phases*

With propel and brake adequately defined, the model is now capable of determining vehicle energy consumption over the City and Highway drive cycles. The final logic included in this model is idle operation. Idle is defined as the periods over a drive cycle when the vehicle is neither accelerating nor moving. During these phases the vehicle is fully at rest and the only power requirement is the accessory load. Therefore, the battery discharge power during all idle phases is taken to be

$$P_{bat}^{idle} = P_{accy} \tag{3.17}$$

where the idle battery power is directly proportional to the vehicle accessory load.. At this point, the vehicle model determines propel battery power for instantaneous propel tractive powers, battery recharge power during braking events, and considers vehicle accessory load during drive cycle idle phases. By applying the bi-directional Willans line introduced in Figure 3.6 and defining the vehicle accessory load, the three distinct drive cycle phases can be modeled on a second by second basis. Figure 3.7 represents how the bi-directional Willans line and idle characteristics are

forged into a 1 Hz vehicle model over the Highway drive cycle. By modeling propel and brake separately the corresponding battery power during each respective phase is discretely determined with the novel bi-directional approach. Figure 3.7 additionally shows the Highway speed profile overlayed with the battery power. Figure 3.8 illustrates the first 505 seconds of the City drive cycle ("505") to more clearly show braking and idle periods. The bi-directional method effectively accounts for propel, brake, and idle phases over a modeled drive cycle.

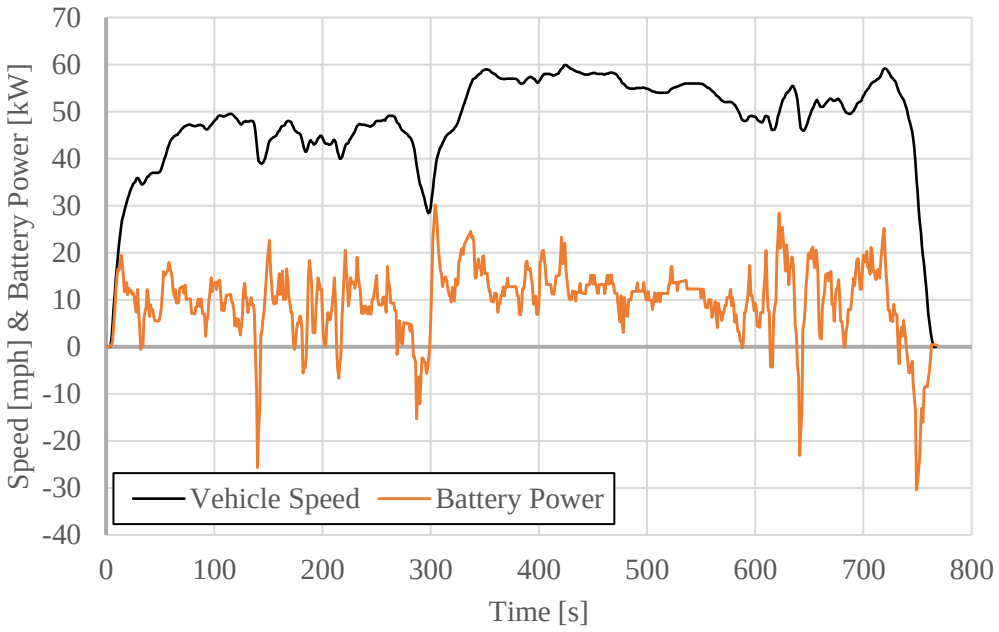

Figure 3.7: *Highway Drive Cycle Speed Profile and Battery Power*

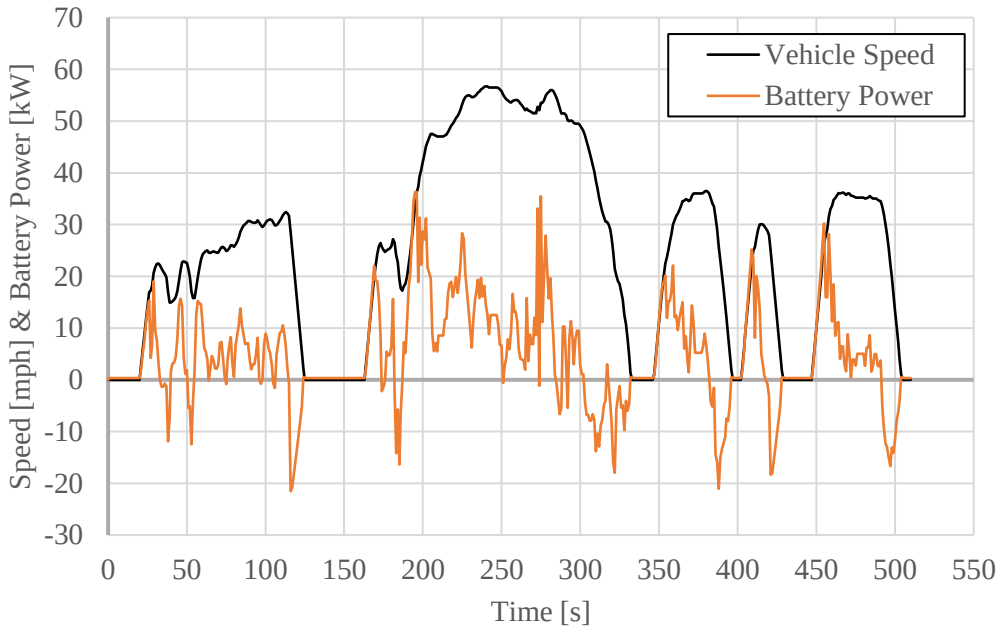

Figure 3.8: *505 Speed Profile and Battery Power*

By modeling the propel, brake, and idle battery power on a 1 Hz basis over a drive cycle the total energy expended during each phase can then be determined. From Equation 3.17 the idle battery energy which is consumed over the drive cycle is governed by the following

$$E_{bat}^{idle} = P_{bat}^{idle} \cdot t_{idle} \tag{3.18}$$

where the energy consumed during idle is directly determined by multiplying the idle battery power by the total idle time. This expression is valid because the idle battery power is a known constant which is always on during idle phases and the idle time is a drive cycle parameter. Applying similar logic for propel ("+") and brake ("-"), the energy consumption for each phase is calculated by

$$E_{bat}^{+/-} = \sum P_{bat}^{+/-} \cdot \Delta t \tag{3.19}$$

where a summation of propel or brake battery power over the entire drive cycle is necessary because the power is determined on a second by second basis. Similar to P_{TR}^{-} and E_{TR}^{-} taking negative values, E_{bat}^{-} also takes negative values. Because 1 Hz drive cycle data is applied, the time

duration of all propel or brake battery power is 1 second which is given generally as Δt above. Applying a bi-directional approach allows the propel and brake energy consumption to be separately determined by the model. With the propel, brake, and idle energy consumption of the vehicle determined the net battery energy consumed over the drive cycle is defined by

$$E_{bat}^{net} = E_{bat}^{+} + E_{bat}^{-} + E_{bat}^{idle} \tag{3.20}$$

where E_{bat}^{net} determined by the model is directly compared to EPA data for tuning the powertrain marginal efficiency, offset, and vehicle accessory load. With the power flow at the battery terminals now defined, all equations up to Equation 3.20 can be integrated into the modeling method to model an electric vehicle powertrain. The subsequent section discusses the process for determining numerous model parameters from EPA test data to enable comparison to model results.

Model Parameter Determination

Model parameter tuning is performed by matching modeled net battery energy consumption to the net battery consumption reported by EPA. City and Highway fuel economy reported in the Application for Certification and Test Car List data sheets are used to determine the vehicle AC energy consumption in Wh/mi of each drive cycle [8][10]. Fuel economy for electric vehicles is stated as miles per gallon equivalent (MPGe). Converting from MPGe to AC electrical energy consumption is done with a 33,700 kWh / gal conversion factor. Thus, the AC energy consumption for a given drive cycle is determined from

$$E_{prim,AC}^{cyc} = \frac{33{,}700\ [AC\ kWh/gal]}{FE\ [mi/AC\ gal\ equiv]} \tag{3.21}$$

where *FE* is the reported fuel economy in MPGe from EPA for a given drive cycle. This conversion is a well-established method and allows the energy consumption of a given drive cycle to be determined. This work focuses on modeling net DC energy consumption of the vehicle, thus converting from AC to DC energy consumption is necessary and done by

$$E_{bat,DC}^{cyc} = E_{prim,AC}^{cyc} \cdot \eta_{chrg} \tag{3.22}$$

where η_{chrg} is the charging efficiency of the battery and $E_{bat,DC}{}^{cyc}$ is the net DC electric energy consumed for the drive cycle. Net energy consumption represents the end of drive cycle phase where the vehicle expends propel energy and recaptures brake energy. Therefore, the proposed model provides a method for accounting for the propel and brake energy consumption to yield a match to EPA reported net energy consumption. This match to EPA reported data is done by effectively modeling the propel, brake, and idle phase losses along with the accessory load and regen fraction to provide additional detail for matching. The charging efficiency represents the losses due to charging the battery, using the onboard vehicle charger, and meeting any accessory load during charging. Therefore, the charging efficiency is separate from the charger efficiency where the latter is simply a ratio of output to input power across the onboard vehicle charger. The charging efficiency can be found by relating the total usable battery capacity to the total recharge event energy such as

$$\eta_{chrg} = \frac{E_{use}}{E_{grid}} \tag{3.23}$$

where E_{grid} is the previously mentioned EPA reported recharge energy necessary to fully recharge the battery system. All batteries are characterized by a maximum energy capacity which is typically reported by manufacturers or found from battery pack design information. The usable capacity E_{use} represents the amount of energy in kWh that can be drained from the battery as

permitted by the control system. Usable energy capacity is not commonly reported by manufacturers but can sometimes be determined from EPA test data. If usable capacity is not reported by the manufacturer, other EPA and third-party sources can be leveraged [12]. Determining the usable capacity of an electric vehicle is important for quantifying the amount of net DC energy consumed by the electric vehicle over a given drive cycle. Validation of the charging efficiency is done by comparing the determined usable capacity to reported maximum capacity and verifying η_{chrg} falls within a reasonable bound of 85-92%. Charging efficiencies outside this bound are taken to be inaccurate and further research is necessary to determine E_{use}. In addition to determining charging efficiency and usable capacity, the vehicle regen characteristics are parameters that must often be estimated. Regen fraction and low-speed cutoff are neither reported nor measured by EPA and are the two key parameters governing regen brake energy capture. For the purposes of this work, the regen fraction and low-speed cutoff are initially taken to be the same for all modeled vehicles. This assumption reduces the number of independent variables and is justified by the low model sensitivity presented in the Sensitivity Analysis section. Additionally, a lumped method is applied to vehicles with multiple motors or all-wheel drive systems for the purpose of developing a single bi-directional Willans line in the absence of possessing detailed information on how either or both motors are operated. Several all-wheel drive vehicles are chosen in this work with the model yielding reasonably accurate results justifying the lumped approach. The final topic is discussing the development of a net Willans line from EPA net energy consumption data for model tuning of the marginal efficiency, offset and vehicle accessory load. The net Willans line is plotted in terms of power such that the battery discharge power is explicitly related to a given tractive power. When converting the EPA reported net energy data to units of power the result is a drive cycle average. EPA reports the net energy consumption

in units of Wh/mi which requires considering the total drive cycle time and distance to convert to units of kW. Therefore, for a specific $E_{bat,DC}^{cyc}$ the conversion to power is given by

$$P_{bat,DC}^{cyc} = \frac{E_{bat,DC}^{cyc} \cdot d_{cyc} \cdot 3.6}{t_{cyc}} \tag{3.24}$$

where d_{cyc} is the drive cycle distance in miles and t_{cyc} is the total drive cycle time in seconds. The factor of 3.6 is to convert from hours to seconds as $E_{bat,DC}^{cyc}$ is in units of Wh/mi. The tractive effort over the drive cycle is also converted to units of power given by

$$P_{TR}^{net} = \frac{E_{TR}^{net}}{t_{cyc}} \tag{3.25}$$

which yields the cycle average tractive power since E_{TR}^{net} is found in the model in units of kJ. An important note to make is each drive cycle results in distinct values of E_{TR}^{net} and P_{TR}^{net}. Therefore, over the City and Highway cycles, two sets of data points are generated which are then plotted to create the net Willans line. This net Willans line is visually comparable to Figure 1.1 and the propel phase of Figure 3.6 as both figures depict a linear Willans line constrained by a set of two operating points. This net Willans line is the primary method by which model results are validated and parameter tuning is performed. The chosen electric vehicles are presented in the Results and Discussion section where a model net Willans line is generated to compare against the EPA net Willans line. Each net Willans line is constrained by a $P_{bat,DC}^{cyc}$ and P_{TR}^{net}. Tuning $slope^{-}$, *offset*, and P_{accy} is performed by matching the model net Willans line to the EPA net Willans line. This tuning method is sufficient for establishing the powertrain parameters and vehicle accessory load.

Chapter 4

Results and Discussion

Selected Vehicles Overview

For the purpose of this work, a total of eight electric vehicles are selected with the proposed modeling method applied. The chosen vehicles are outlined in greater detail in Table 4.1 with model years ranging from 2016 to 2021. A mixture of sedans, SUVs and performance vehicles are chosen to encapsulate all ends of the electric vehicle market. Additionally, two older model year vehicles are selected because no powertrain changes were made between the chosen year and newer models. Changes to a vehicle powertrain is captured by the EPA reported vehicle ID and the tested vehicle model year. Lastly, the selected vehicles are also chosen to represent a broad range of test mass, motor power, battery capacity, and drivable range. The data contained in Tables 4.1 and 4.2 stems from Application for Certification and Certification Summary Information published by the EPA. Table 4.2 contains measured test data and calculated information for each vehicle when driven over the Multi-Cycle Test (MCT). The MCT is a drive cycle comprised of varying UDDS and HWFET portions with constant speed intervals to deplete the battery system [13]. The information contained in Table 4.2 includes the energy consumption to recharge the battery, the estimated charging efficiency, the unadjusted fuel economy, and the label vehicle range. The label range is adjusted from the EPA reported energy consumption and reported on fueleconomy.gov [12]. Key selected vehicles include the 2019 Tesla Model X Long Range, as Tesla arguably comprises a significant portion of the electric vehicle market today. Tesla vehicles have become increasingly popular due to the significant driving range, acceleration performance, and overall efficiency. The 2020 Porsche Taycan Turbo is a performance sedan which features a significantly high nominal voltage battery system which allows for quick recharging and high

operating motor speeds. The 2017 BMW i3 is selected as this vehicle represents a smaller and highly efficient electric vehicle intended as a commuter vehicle. Lastly, the 2016 Nissan Leaf is chosen to represent an early electric vehicle with less developed technology compared to current vehicles. The results presented are centered on these chosen vehicles.

Table 4.1: *Selected Electric Vehicles for Model Analysis*

Model	Driven Axle	Test Mass	Motor Power	Usable Energy	Battery Capacity	Nominal Voltage
		[kg]	[kW]	[kWh]	[Ah]	[V]
2017 BMW i3	RWD	1474	125	29.3	94	360
2020 Chevrolet Bolt	FWD	1758	150	66	189	400
2021 Ford Mach-E Stand. Range	RWD	2155	198	68	216	350
2021 Ford Mach-E Ext. Range	RWD	2268	216	88.5	288	342
2019 Jaguar I-Pace	4WD	2268	294	87.6	223	400
2016 Nissan Leaf	FWD	1701	80	27.9	83	361
2020 Porsche Taycan Turbo	AWD	2495	290	83.7	129	724
2019 Tesla Model X Long Range	AWD	2722	398	98	250	400

Table 4.2: *Vehicle Energy Consumption and Charging Metrics with Label Range*

Model	Recharge Event	Charging Eff.	City		Highway		Label Range
			Fuel Economy	Energy Consumption	Fuel Economy	Energy Consumption	
	[AC kWh]	[%]	[MPGe]	[DC Wh/mi]	[MPGe]	[DC Wh/mi]	[mi]
2017 BMW i3	32.3	90.7%	184	166	152	201	114
2020 Chevrolet Bolt	73.6	89.7%	182	166	154	197	259
2021 Ford Mach-E Stand. Range	77.6	87.6%	147	201	131	226	230
2021 Ford Mach-E Ext. Range	102	87.2%	146	201	127	231	300
2019 Jaguar I-Pace	104	84.2%	115	247	104	274	234
2016 Nissan Leaf	31.8	87.8%	177	168	145	205	107
2020 Porsche Taycan Turbo	98.1	85.4%	96.9	297	102	284	201
2019 Tesla Model X Long Range	115	85.4%	132	218	125	231	325

Vehicle Model Results

Each vehicle from Table 4.1 is modeled individually against available net battery energy consumption for the City and Highway cycles. Note that net consumption is used to tune and fit the model as net data is the only available information reported by EPA. Utilizing the modeling methods, the powertrain parameters are then derived and tuned to achieve a fit with EPA test data. Table 4.3 contains 2017 BMW i3 net tractive energy for the City and Highway drive cycles, with the net battery consumption from Table 4.2 repeated for ease of comparison. The metrics reported in Table 4.3 are directly used by the model to generate powertrain marginal efficiency, offset, accessory load, and regen fraction estimates. Additionally, as will be discussed later, the net energy values in Table 4.3 are used to derive the net Willans line. The proposed methodology for estimating the powertrain parameters, vehicle accessory load, and regen fraction is through matching the model net Willans line to the EPA net Willans line. Thus, the model net Willans line is matched to the Willans line derived from the data presented in Table 4.3.

Table 4.3: *2017 BMW i3 City and Highway Net Energy Demand*

2017 BMW i3	City	Highway
	[DC Wh/mi]	[DC Wh/mi]
Net Tractive Energy	113	173
Net Battery Energy	166	201

To better illustrate how the net battery consumption is determined from the model, Table 4.4 contains data from the same 2017 BMW i3 but with the modeled propel, brake and idle energy consumption for the City and Highway cycles. For conveying how net energy consumption is determined through the model, units of Wh/mi are shown in Table 4.4. Later in the results section units of power will be used moving forward. Table 4.4 helps illustrate how the propel, brake, and idle energy consumptions are summed together to yield the net values which are reported by EPA.

Tuning the powertrain parameters and vehicle accessory load leads to the propel, brake, and idle energy consumption results in Table 4.4. Agreement between the model net Willans line and EPA net Willans line is achieved when the propel, brake, and idle energy consumption converges to net values by iterating the powertrain parameters and vehicle accessory load. Because the degrees of freedom of the model exceed the data points available, no solution achieved is considered unique. The powertrain marginal efficiency, offset, and vehicle accessory load are all tuned such that the model net Willans line matches the EPA net Willans line. Because three independent variables are tuned, multiple solutions exist for a single vehicle. The inability to achieve a unique solution is not disparaging towards the modeling method as the powertrain parameters determined by matching net Willans lines leads to reasonably accurate results, as is shown in this section and further proven in the Sensitivity Analysis section. The model shows reasonable resiliency to changes in input parameters as is discussed further in the Results and Discussion section.

Table 4.4: *2017 BMW i3 Modeled Propel, Brake and Idle Energy Demand*

2017 BMW i3	City	Highway
	[DC Wh/mi]	[DC Wh/mi]
Propel Tractive Energy	198	190
Propel Battery Energy	228	215
Regen Tractive Energy	-77.3	-16.4
Regen Battery Energy	-65.2	-14.1
Idle Accessory Energy	2.87	0.03
Net Battery Energy	166	201

Moving on from the motivation for matching net Willans lines between the model and EPA, the process for determining powertrain parameters and vehicle accessory load is discussed. As Table 4.2 – 4.4 illustrated, the process of flowing from derived net EPA test data to separating propel, brake, and idle energy consumption is relatively straightforward. With the three operational states broken out by the model the powertrain parameters and vehicle accessory load

are tuned. Table 4.5 contains derived net Willans line parameters for each of the chosen vehicles. Figure 4.1 contains the derived net Willans line for the 2017 BMW i3 from reported EPA data, which helps illustrate how the net marginal efficiency and offset are derived from the two drive cycle data points. For clarity and the sake of differentiating, the net marginal efficiency is referred to as ME_{net} and is derived from a simple inverse slope calculation. The net offset is referred to as $offset_{net}$ and is determined by subtracting the net battery power by the net slope multiplied by the net tractive power for a drive cycle. The net Willans line and accompanying parameters relate power flow from the battery terminals to power demand at the wheels for drive cycle average powers. As was illustrated in Figures 3.2 – 3.4, the regen characteristics and accessory load are intrinsically coalesced into ME_{net} and $offset_{net}$. To this end, the net Willans line is not wholly representative of the vehicle powertrain efficiency. The net Willans line instead represents how the vehicle as a system meets a drive cycle average tractive power and necessary accessory load. Utilizing units of power lends advantages as $offset_{net}$ is directly calculated as a loss term. The net offset can be interpreted as the vehicle overhead power necessary for operating the powertrain and meeting accessory load. Units of power are presented moving forward in the results section because the net offset can be represented as a loss term. Converting between power and energy can easily be done by considering the drive cycle time and distance. As a final note, results presented in terms of power or energy leads to no change with the assertions made or results gathered. Therefore, analyzing vehicles on a power or energy basis provides different use cases.

Table 4.5: *Derived Net Willans Line Parameters for Modeled Vehicles*

Model	Net Marg. Eff. [%]	Offset Net [kW]
2017 BMW i3	94.75	0.912
2020 Chevrolet Bolt	101.6	1.121
2021 Ford Mach-E Stand. Range	96.71	1.484
2021 Ford Mach-E Ext. Range	95.66	1.400
2019 Jaguar I-Pace	98.24	1.864
2016 Nissan Leaf	98.81	1.056
2020 Porsche Taycan Turbo	92.00	2.504
2019 Tesla Model X Long Range	104.3	1.662

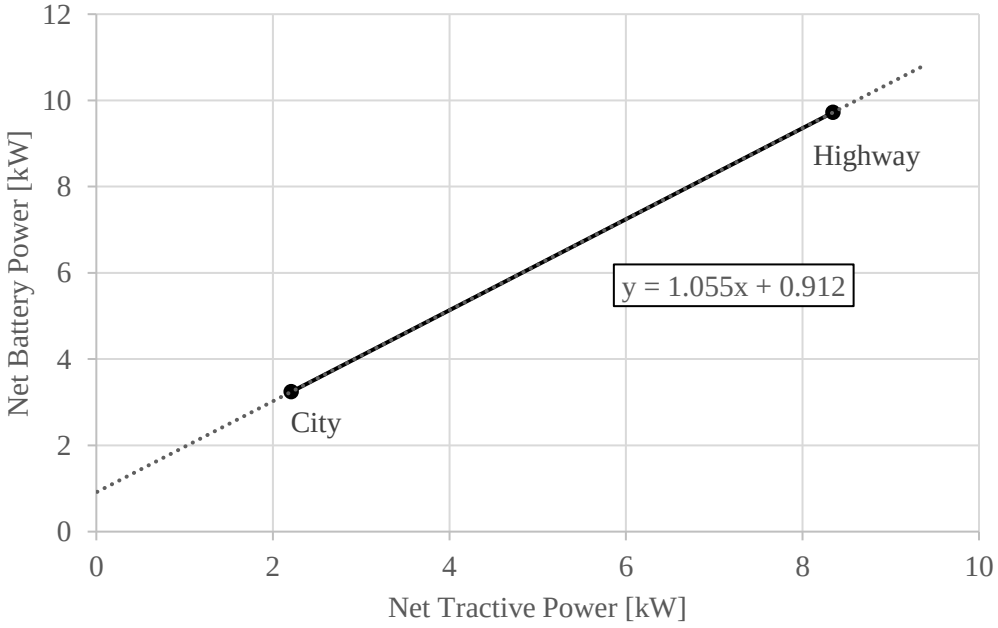

Figure 4.1: *2017 BMW i3 Derived Net Willans Line Plotted for Two Drive Cycles*

An interesting property of two of the eight vehicles is illustrated when plotting on a net power basis where ME_{net} exceeds 100% as shown in Table 4.5. This phenomenon is not a concern to the proposed modeling method for several reasons. First, ME_{net} purely relates cycle average battery power to a cycle average tractive power, therefore a value of ME_{net} greater than 100% does not imply an efficiency greater than unity. As was initially discussed, a marginal efficiency purely represents a linear or stepped change between one data point to the next. Therefore, the marginal

efficiency is not solely reflective of the efficiency. Second, and most important, vehicle regenerative braking characteristics vary vehicle to vehicle. As is discussed later in this work, a constant low-speed cutoff and regen fraction is applied to all vehicles, but for vehicles with values of ME_{net} over 100% a lower regen fraction is applied. Regenerative braking potential is most abundant over drive cycles with ample braking opportunities. Therefore, the City drive cycle energy consumption is most affected by the regenerative braking parameters selected and can correspondingly affect the net marginal efficiency. The phenomenon of ME_{net} being greater than unity is taken to be indicative of a vehicle with less regenerative braking capture. Vehicles with less regenerative braking capture will have higher City drive cycle energy consumption which translates to increased battery consumption. Increasing just the City point decreases the net Willans line slope and subsequently increases the marginal efficiency. Ultimately, a ME_{net} which exceeds 100% is of no concern to the proposed modeling method.

From the net Willans line parameters presented in Table 4.5 and the corresponding net tractive effort relationship illustrated in Figure 4.1, the powertrain parameters are then investigated. The powertrain parameters are tuned to match the net Willans line like Figure 4.1. Table 4.6 contains the corresponding powertrain marginal efficiency, offset, vehicle accessory load and the regen fraction as determined by matching the EPA net Willans line. All vehicles are modeled with a low-speed cutoff of 5 mph and a regen fraction of 94%, unless otherwise specified. The motivation for selecting 5 mph as the cutoff and 94% as the regen fraction stems from the major results presented in [14][15]. Several hybrid electric vehicles are tested on chassis dynamometers with the total braking force and regen braking force recorded over the City and Highway drive cycles in [14]. Older model year hybrid vehicles were tested in [14] but the major results presented illustrate a significant availability of regenerative braking energy over mild drive

cycles. This takeaway is seen from the majority of braking force being captured by the regenerative braking system. Additionally, all vehicles cut regen braking when operated at speeds below 5 mph. These two major results provide justification for setting the regen brake faction to 94% and ceasing all regen braking at speeds below 5 mph. The work performed in [15] is centered around developing a regenerative braking strategy for vehicle implementation. The major results contained in [15] depict regen braking ceasing at low speeds below 10 mph, typically around 5 – 7 mph. From the results presented in [14][15] the justification for selecting 94% and 5 mph as the appropriate regen characteristics is provided. With modern electric vehicles containing larger battery systems and more powerful motors, modern electric vehicles are less likely to be hardware limited when performing regen braking. These hardware limits correlate to regen braking torque and motor current being of less concern when compared to earlier electric vehicles. Modern electric vehicles are typically physics limited with regards to the amount of regen braking possible as drivability and safety must be maintained. With the work presented in [14][15] and the current trends of electric vehicles, the regen estimations applied in this work are justified.

Table 4.6: *Established Powertrain Parameters for Modeled Vehicles*

Model	Marginal Eff.	Offset	Accessory Load	Regen Fraction
	[%]	[W]	[W]	[%]
2017 BMW i3	92.0	143	315	94
2020 Chevrolet Bolt	97.7	160	351	80
2021 Ford Mach-E Stand. Range	94.9	650	410	94
2021 Ford Mach-E Ext. Range	92.0	246	410	94
2019 Jaguar I-Pace	97.5	790	831	94
2016 Nissan Leaf	97.0	184	585	94
2020 Porsche Taycan Turbo	89.0	900	738	94
2019 Tesla Model X Long Range	98.3	173	343	75

Insight to the powertrain characteristics of each modeled vehicle is enabled from this modeling method as illustrated by the results in Table 4.6. The 2019 Tesla Model X Long Range

achieved the greatest marginal efficiency and is therefore the most effective vehicle at converting battery power to tractive power. The Tesla was also modeled with the lowest regen fraction of all the vehicles but is due to the Tesla having the largest ME_{net}. Both the Jaguar and Porsche experience reasonably high powertrain offsets and vehicle accessory loads. Both the Jaguar and Porsche are relatively heavy vehicles with dual motor designs modeled as a lumped system. Therefore, the total offset would realistically be divided amongst each individual motor system versus a single powertrain having an unreasonably high offset. Lastly, both vehicles are modeled with the largest accessory loads but with values remaining within reasonable limits. Therefore, the powertrain and vehicle parameters are considered representative of both vehicles.

The parameters presented in Table 4.6 lend insight directly to the vehicle powertrain.. Additional vehicle information is derived from tuning the model to achieve a fit with net EPA test data for the City and Highway drive cycles. The ability of the model to estimate vehicle energy consumption for drive cycles beyond the City and Highway cycles is also considered. By taking the parameters derived from the City and Highway cycles, a battery energy consumption can be determined for any drive cycle. To explore this question, the Tesla is run over the US06 City and Highway drive cycles which are considered significantly more 'aggressive' cycles. The Tesla is chosen as the manufacturer reports US06 energy consumption data for select models within the Application for Certification data. The availability of this data allows model results to be directly compared. Table 4.7 contains energy consumption data reported by both EPA and Tesla for the certification cycles and the US06 City and Highway cycles. From Table 4.7 the increased drive cycle demand for the US06 cycles is illustrated as the energy consumption is significantly higher. The aggressive US06 cycles provide an additional method for verifying the results gathered by the EPA net Willans line for the certification cycles. Table 4.8 presents the results of modeling the

Tesla over the US06 cycles with parameters determined from the City and Highway cycles. The percent difference between the model results and the reported test data is also included. From the results of Table 4.8, the model provides reasonable results for the US06 cycles when using the powertrain parameters derived from the City and Highway cycles. The results in Table 4.8 validate and provide justification for the tuning method proposed. Matching both net Willans lines to establish powertrain parameters is an effective strategy and can be extrapolated with reasonable results to other drive cycles. The powertrain parameters established by the proposed method are considered representative of the vehicle because of the low percent difference between measured test data and modeled results.

Table 4.7: *2019 Tesla Model X Long Range US06 Energy Consumption*

2019 Tesla Model X Long Range	Fuel Economy	Energy Consumption
	[MPGe]	[DC Wh/mi]
City	132	218
Highway	125	231
US06 City	81.6	353
US06 Highway	94.6	304

Table 4.8: *2019 Tesla Model X Long Range Modeled US06 Consumption*

2019 Tesla Model X Long Range	Modeled Consumption	Percent Difference
	[DC Wh/ mi]	[%]
US06 City	357	1.14%
US06 Highway	316	3.83%

With the availability of US06 drive cycle data a three point fit is explored to investigate deriving a better fit for vehicle parameters. From the results presented in Tables 4.7 & 4.8, the Tesla powertrain parameters are re-tuned by adding the US06 operating points onto the net Willans line plot. For the sake of convenience, the US06 City and Highway points are combined into a single US06 drive cycle point. The US06 is the encapsulating drive cycle which contains the city

and highway portions. Therefore, combining the two US06 points is possible and combining the points is done to model the entire drive cycle. The addition of a third operating point translates to the net Willans line no longer being constrained strictly by the UDDS and HWFET drive cycle points. An R^2 value is introduced to the fitting method to ensure the model net Willans line most effectively matches the EPA net Willans line. Table 4.9 contains the ME_{net}, net offset, and R^2 values for each of the net Willans lines according to the fit method. The R^2 value represents how well the net Willans line fits the operating points with respect to the powertrain parameters. A major difference with adding the third operating point is ME_{net} being less than 100%. With the addition of the US06 data, the slope of the net Willans line becomes greater than unity. The net offset additionally decreases from 1.662 kW to 1.117 kW, a drop of 0.545 kW. Table 4.10 contains the original powertrain parameters established from the two point method, and the re-tuned parameters using the three point method. Immediately an increase of the regen fraction by 10% is shown and an increase of the accessory load by about 320 W is determined, these changes correlate to a percent difference of +11.8% and +48% respectively. The powertrain marginal efficiency and offset remain relatively constant with the accessory load and regen fraction being the primary tuning parameters. Although the accessory load and regen fraction change by noteworthy amounts, the rather insignificant changes in powertrain marginal efficiency and offset are expected. As is discussed in the Sensitivity Analysis section, the model is fairly sensitive to changes in accessory load and very resilient to changes in regen fraction. The accessory load affects all operating points equally because the load is always on. Therefore, the accessory load can be used as a final tuning method to reach net offset agreement. Because ME_{net} decreases to less than 100%, the regen fraction can be increased to more accurately represent the regen fraction of the vehicle. In conclusion, additional operating points help further constrain the model and lead

to more representative powertrain parameters being derived, however the obtained solution is still not unique as the number of independent variables still exceed the number of data points.

Table 4.9: *Tesla Net Willans Line Parameters for Different Fit Methods*

2019 Tesla Model X Long Range	Net Marg. Eff.	Offset Net	R^2 Value
	[%]	[kW]	[%]
2 Point Method	104.3	1.662	100
3 Point Method - EPA	91.9	1.117	98.6
3 Point Method - Model	91.9	1.118	98.9

Table 4.10: *Tesla Powertrain Parameters for Different Fit Methods*

2019 Tesla Model X Long Range	Marginal Eff.	Offset	Accessory Load	Regen Fraction
	[%]	[W]	[W]	[%]
2 Point Method	98.3	173	343	75
3 Point Method	98.4	164	660	85

Powertrain Efficiency

Establishing representative powertrain parameters from the City and Highway drive cycles by matching the EPA net Willans line is shown to be an effective strategy for tuning the model. The results previously presented illustrated the accuracy and capability of the model for identifying detailed vehicle information from EPA net energy consumption test data and applying a bi-directional Willans line. The marginal efficiency of the vehicle is not wholly reflective of the powertrain efficiency. The offset must be used in conjunction with the marginal efficiency to determine the efficiency. The efficiency of a component or system is taken to be the ratio of output power to input power. In terms of the applied linear approximation, the input power is established by the following

$$P_{in} = P_{out} \cdot slope + offset \tag{4.1}$$

where P_{out} has been correlated to tractive effort at the wheel. More broadly, the output power of a powertrain can be taken as the gearbox output power for a given torque and speed load. With this definition in mind and applying the established parameters presented in Table 4.6, the powertrain efficiency can be determined from the model. Isolating the vehicle powertrain from other losses is important for representing how the vehicle powertrain converts battery discharge power to gearbox output power. In other words, isolating the vehicle powertrain from regen characteristics and accessory load is necessary. As there are separate propel and brake slopes, the model provides a method for determining a powertrain propel or brake efficiency. Determining the propel efficiency of the 2017 BMW i3 is discussed in this section. Figure 4.2 illustrates the propel battery power (input) for corresponding propel tractive power (output) for typical ranges observed over the City and Highway cycles. Only propel is illustrated in this section, but braking follows a similar trend. With the tractive power known, the corresponding motor power is calculated from the powertrain parameters presented for the 2017 BMW i3 in Table 4.6. As is expected, lowest efficiency occurs at the lowest output powers with efficiency increasing as load increases. This relationship is expected because the constant offset has less of an impact at higher loads than at lower loads. Additionally, because the offset is on the order of magnitude of watts, the vehicle powertrain quickly reaches the efficiency limit of 92% as established by the marginal efficiency.

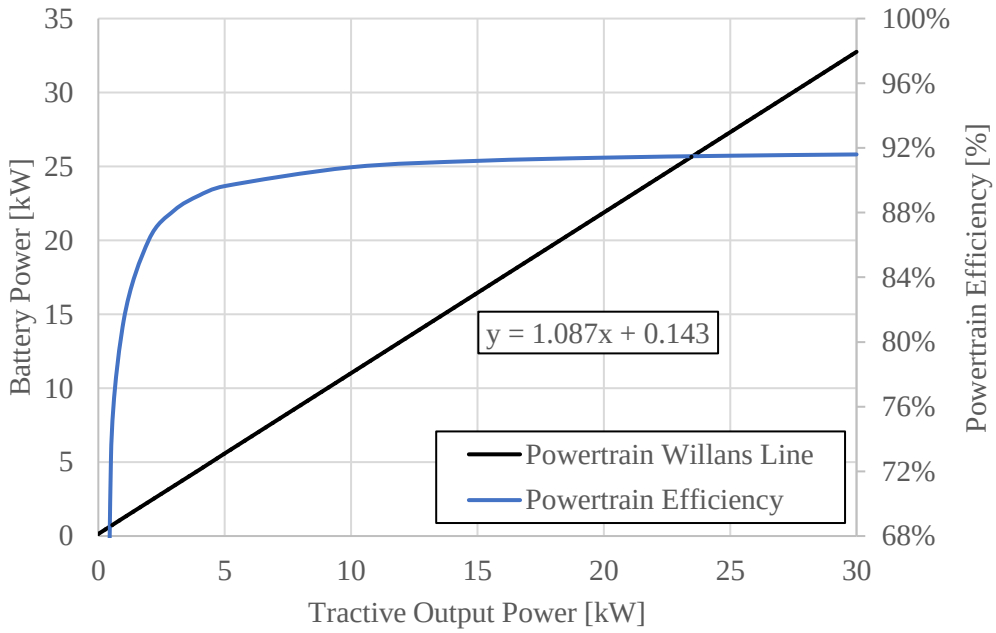

Figure 4.2: *2017 BMW i3 Propel Efficiency Curve from Established Parameters*

To briefly note, the efficiency curve presented in Figure 4.2 is fairly simplistic as the powertrain efficiency is derived from the linear Willans line model. As such, this efficiency approximation would likely deviate from the true powertrain efficiency at higher loads due to the linear nature of the model. Despite the simplified efficiency curve, the results of Figure 4.2 are taken to be representative of the powertrain since the majority of driving does not occur at peak operating limits. Deriving powertrain efficiency from the use of EPA vehicle data and applying a bi-directional Willans line is greatly useful. Operating characteristics of the vehicle powertrain can be determined from the use of a linear approximation; no detailed information is necessary for determining powertrain efficiency at varying loads. The proposed modeling method therefore enables determining powertrain characteristics beyond vehicle energy consumption.

Model Sensitivity Analysis

The final discussion is on the sensitivity of the proposed modeling method when changes to the input parameters occur. Due to the degrees of freedom of the model, a solution cannot be stated as unique as multiple combinations of input parameters can yield a fit to EPA data. Using public test data as the sole means of data collection is an attractive attribute of the proposed method. However, there is possibility for reported data to be incorrect or wrongly reported. Additionally, information reported in the Application for Certification data is not labeled as continuous, peak, usable or rated so reasonable assumptions must be made. Therefore, distilling information reported by EPA can present a challenge when listed information is mislabeled or units are not given. With these challenges presented, understanding how resilient the model is to changes in vehicle data and model inputs is of great interest. Characterizing the model sensitivity to changes in the inputs provides knowledge into the fidelity of generated powertrain parameters. To this end, the sensitivity of the model is investigated with respect to each of the four main inputs: powertrain marginal efficiency, powertrain offset, accessory load, and regen fraction.

To enable the sensitivity study, a transfer function relating input and output parameters is of high value. Due to the linear nature of the model, an expression for cycle average net battery power is obtained. The net Willans line for the vehicle is derived from EPA test data and tractive effort, therefore the cycle average net battery power is related to the following

$$P_{bat}^{net} = \frac{P_{TR}^{net}}{ME_{net}} + offset_{net} \tag{4.2}$$

where the cycle average net battery power is determined from the net Willans line parameters. There is great use in Equation 4.2, however the model input parameters are not explicitly included within the expression. By applying Equations 3.14, 3.16 & 3.17 an expression relating cycle

average net battery power to the major model inputs is derived. Equations 3.14, 3.16 & 3.17 govern the instantaneous power flow during a drive cycle. To convert these equations to represent drive cycle averages the total power must be summed over the drive cycle to yield energy, and then divided by total cycle time to yield average power. By considering drive cycle time and regen characteristics the following transfer function is derived

$$P_{bat}^{net} = \frac{P_{TR}^{+}}{slope^{-}} + \alpha \cdot RF \cdot (P_{TR}^{-}) \cdot slope^{-} + \beta \cdot offset + P_{accy} \tag{4.3}$$

where Equation 4.3 is now explicitly in terms of the major model inputs. The newly established terms α and β are drive cycle dependent constants which are fit from vehicle averages for all eight vehicles. The constant α represents the percentage of braking events where energy is recaptured by the motor system. Therefore, α encapsulates the times when the low-speed cutoff is enforced and the vehicle brakes but no regen energy is captured. The regen fraction multiplied by α represents what is referred to in this work as the *capture ratio CR*. The capture ratio represents the energy ratio that is captured and used for regen to the total braking energy for a specific drive cycle. Written explicitly, alpha can be determined from the following

$$\alpha = \frac{E_{regen}}{E_{TR}^{-}} \tag{4.4}$$

where E_{regen} is the summation of all regenerative braking power over a drive cycle multiplied by the time step. In this work all time steps are equal to 1 second. The constant β represents the percentage of the drive cycle in which the vehicle is meeting a speed demand, or written explicitly

$$\beta = \frac{t_{cyc} - t_{idle}}{t_{cyc}} \tag{4.5}$$

Therefore, the percentage of idle time for a drive cycle can be determined by subtracting β from unity. As was previously mentioned, α is an average across all modeled vehicles for the City and Highway cycles for each of the eight modeled vehicles which is done to establish α and β as constants in Equation 4.3. The justification for establishing α and β as constants is leveraged by the fact the idle time and capture ratio vary minimally between all eight vehicles. Therefore, α and β take on the values contained in Table 4.11. With Equation 4.3 derived and values for α and β outlined, the sensitivity of the model can be determined by differentiating Equation 4.3 with respect to each model input parameter. This section discusses the gathered results for the sensitivity of the model with respect to the marginal efficiency, offset, accessory load, and regen fraction for the 2017 BMW i3.

Table 4.11: *Values of Drive Cycle Dependent Constants α and β*

Drive Cycle	α [/]	β [/]
City	0.972	0.822
Highway	0.995	0.995

Powertrain marginal efficiency is the first model input evaluated for sensitivity. By taking the derivative of Equation 4.3 with respect to each model input, while holding all else constant, the respective change in cycle average net battery power for a change in a parameter is determined. Therefore, the first derivative of Equation 4.3 with respect to marginal efficiency yields the following

$$\frac{dP_{bat}^{net}}{dslope^{-}} = \alpha \cdot RF \cdot P_{TR}^{-} - \frac{P_{TR}^{+}}{slope^{-\,2}} \tag{4.5}$$

where a non-linear relationship between changes in marginal efficiency and cycle average net battery power is found. This relationship is to be expected as the marginal efficiency is always

less than unity, so increases in marginal efficiency will cause the result of Equation 4.5 to decrease. Therefore, increases in marginal efficiency subsequently decrease the required cycle average net battery power. An interesting characteristic of Equation 4.5 is the presence of a limit. The marginal efficiency of a component cannot physically exceed unity, but an increasingly positive value of marginal efficiency drives Equation 4.5. to a value of $\alpha(RF)P_{TR}^{-}$. Conversely, decreasing marginal efficiency will drive Equation 4.5 to negative infinity. Equation 4.5 can be plotted to visualize the relationship between changes in cycle average net battery power to changes in marginal efficiency, but what is arguably more useful is visualizing the change in cycle average net battery power entirely. Figure 4.3 contains the change in cycle average net battery power for changes in marginal efficiency with respect to the established powertrain parameters in Table 4.6. Since Equation 4.5 is in terms of finite quantities, the original value of marginal efficiency must be considered when studying how a new value of marginal efficiency affects cycle average net battery power. Figure 4.3 illustrates the change in cycle average net battery power for marginal efficiencies between 60% and 100%. Electric vehicle powertrains are more efficient and effective than conventional powertrains at converting input power to meet tractive effort demand. Therefore, 60% marginal efficiency is considered very low and not representative of any production electric vehicle. Conversely, a marginal efficiency greater than 99% is likely too high and not representative of a production vehicle. Therefore, the range of 60% to 100% marginal efficiency is chosen to encapsulate both ends with expected values of marginal efficiency lying between 86% and 98%.

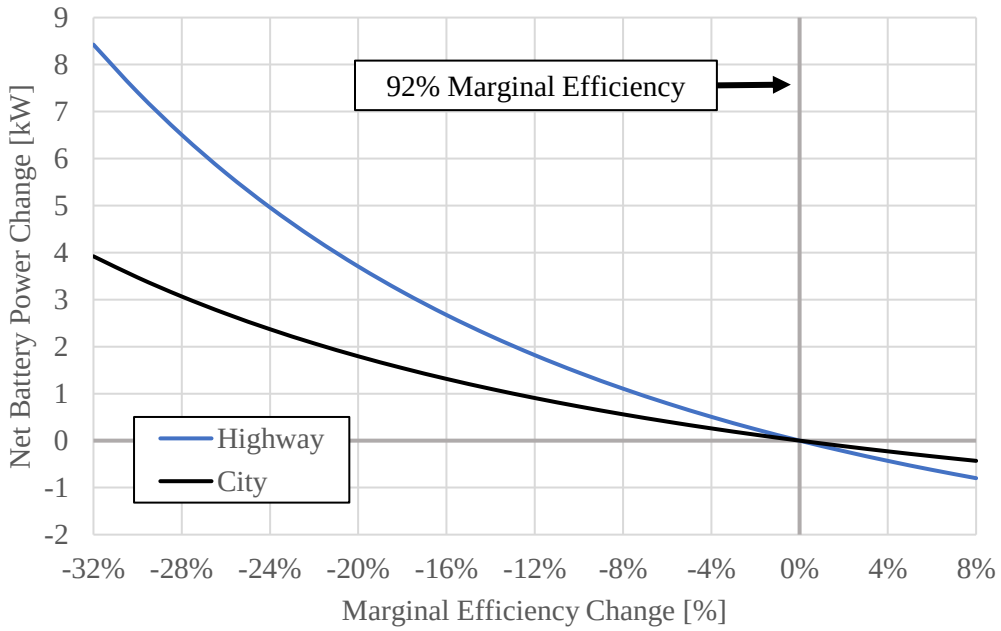

Figure 4.3: *Net Battery Power Change for Finite Changes in Marginal Efficiency*

From Figure 4.3 the sensitivity of each drive cycle, and the model as a whole, is captured. The Highway cycle is more sensitive to changes in marginal efficiency than the City cycle. This trend is to be expected as the Highway cycle has a greater average speed and greater tractive effort demand than the City cycle. Because of these Highway cycle characteristics, the cycle average net battery power over the Highway cycle is more sensitive to changes in the marginal efficiency. Figure 4.4 illustrates the new cycle average net battery power for corresponding marginal efficiencies. The dashed and labeled line represents the marginal efficiency established for the vehicle. From the results presented in Figure 4.3, and the trends shown in Figure 4.4, the closer the marginal efficiency is to 100% the less the cycle average net battery power becomes. For reasonable values of marginal efficiency ranging from 86% to 98%, the model is fairly resilient. Table 4.12 contains cycle average net battery power values for the finalized model and for marginal efficiencies of 86% and 99% for each drive cycle. With Figure 4.4 and Table 4.12 illustrating how the cycle average net battery power changes according to a set marginal efficiency, Figure 4.5

illustrates how the net Willans line changes. Figure 4.5 contains net Willans line plots for marginal efficiencies of 86%, 99% and the original value of 92% (shown in black). With changes in marginal efficiency both ME_{net} and $offset_{net}$ change accordingly. As powertrain marginal efficiency increases both ME_{net} and $offset_{net}$ decrease. Since the net Willans line is used to tune the input parameters, Figure 4.5 more effectively illustrates the sensitivity of the model to changes in powertrain marginal efficiency and the justification for the model being deemed fairly resilient. With additional vehicle data the powertrain marginal efficiency can be more accurately determined, however the proposed method works reasonably well with establishing powertrain marginal efficiencies from public test data.

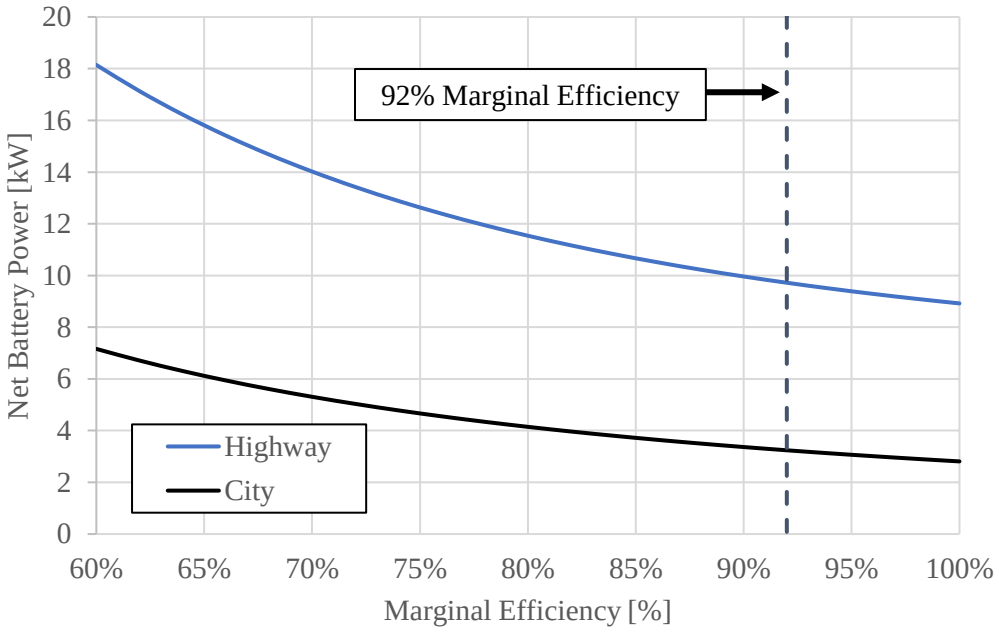

Figure 4.4: *New Cycle Average Net Battery Power for Specific Marginal Efficiencies*

Table 4.12: *2017 BMW i3 Sensitivity to Changes in Marginal Efficiency*

Powertrain Marginal Efficiency	City		Highway	
	Power Change [kW]	Net Battery Power [kW]	Power Change [kW]	Net Battery Power [kW]
86%	0.404	3.64	0.793	10.51
92%	0	3.24	0	9.72
99%	-0.382	2.86	-0.712	9.01

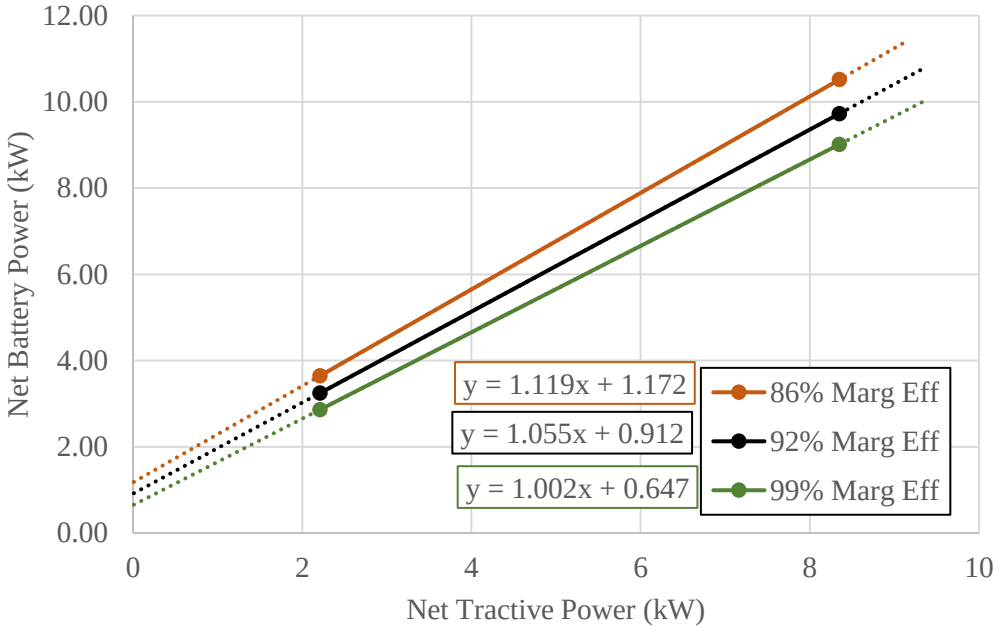

Figure 4.5: *Model Sensitivity to Powertrain Marginal Efficiency*

With the model sensitivity to changes in marginal efficiency presented, the powertrain offset is evaluated. As with Equation 4.5, the derivative of Equation 4.3 is derived with respect to only the powertrain offset. Performing this derivative yields the following sensitivity expression

$$\frac{dP_{bat}^{net}}{dOffset} = \beta \tag{4.6}$$

where a constant relationship between changes in powertrain offset and the cycle average net battery power is observed. Therefore, for changes in the powertrain offset, the cycle average net battery power will change by a factor of β multiplied by the offset change. Just as with the

sensitivity to marginal efficiency, Figure 4.6 illustrates the cycle average net battery power change for changes in the powertrain offset. The slope of each line in Figure 4.6 is equivalent to the drive cycle constant β previously introduced. Similar to changes in the marginal efficiency, the Highway cycle is more sensitive to changes in the powertrain offset than the City cycle. Because the highway has less idle periods than the City cycle, the β value for the Highway is greater and correlates to the powertrain offset impacting the cycle average net battery power more than over the City cycle. Figure 4.7 illustrates new cycle average net battery powers for the corresponding change in the powertrain offset. Ranges of 0 kW to 1 kW are considered for the powertrain offset as power losses over 1 kW are unexpected and likely to be non-representative of electric vehicles. Table 4.13 contains discrete cycle average net battery power values for a powertrain offset of 0 kW and 1 kW. Across this wide range of offset values, there is minimal change in the cycle average net battery power. Figure 4.8 illustrates how the net Willans line changes according to changes in offset; for clarity the 0 W offset curve is not plotted. As is to be expected, as the powertrain offset increases ME_{net} and $offset_{net}$ also increase. Therefore, the model shows increased resiliency to changes in the powertrain offset, yielding high confidence in the chosen powertrain offset. To conceptualize, an increase of powertrain offset to 1 kW is a 700% increase for the BMW i3. This offset increase only translates to a City cycle average net battery power of 3.94 kW which is a percent increase of only 21.6%. From these results, the model is asserted as reasonably resilient to changes in powertrain offset which correlates to the modeling method establishing representative values of powertrain offset.

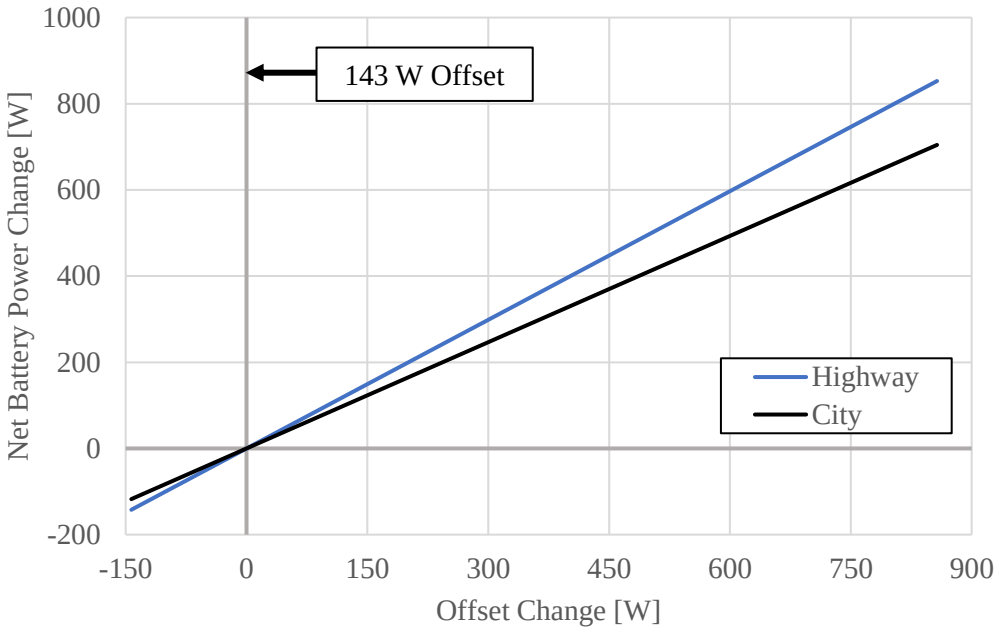

***Figure 4.6**: Net Battery Power Change for Finite Changes in Offset*

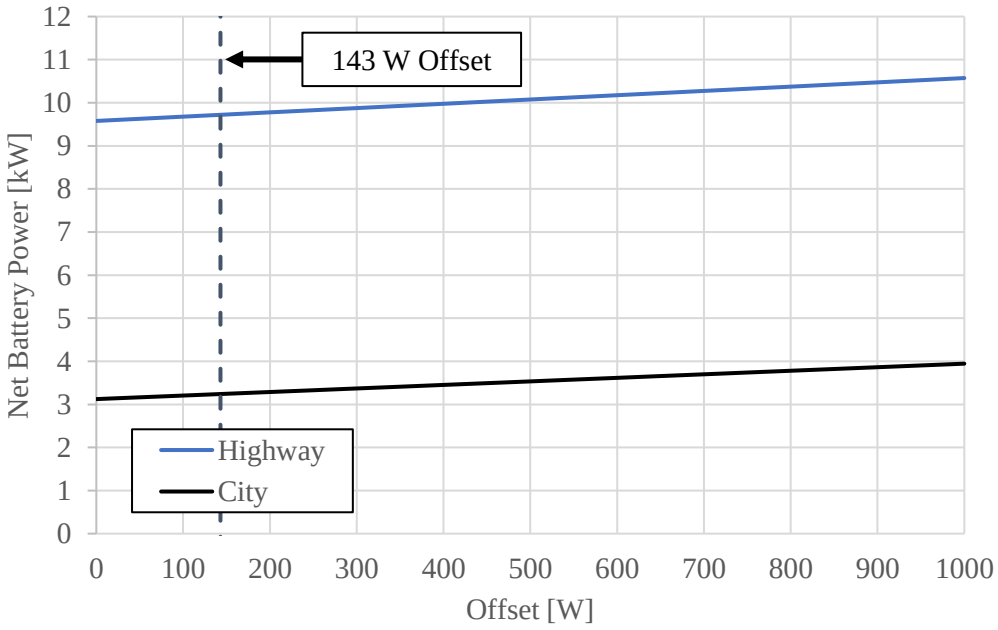

***Figure 4.7**: New Cycle Average Net Battery Power for Specific Offsets*

Table 4.13: *2017 BMW i3 Sensitivity to Changes in Offset*

Powertrain Offset	City		Highway	
	Power Change	Net Battery Power	Power Change	Net Battery Power
[W]	[W]	[kW]	[W]	[kW]
0	-118	3.12	-142	9.58
143	0	3.24	0	9.72
1000	704	3.94	853	10.6

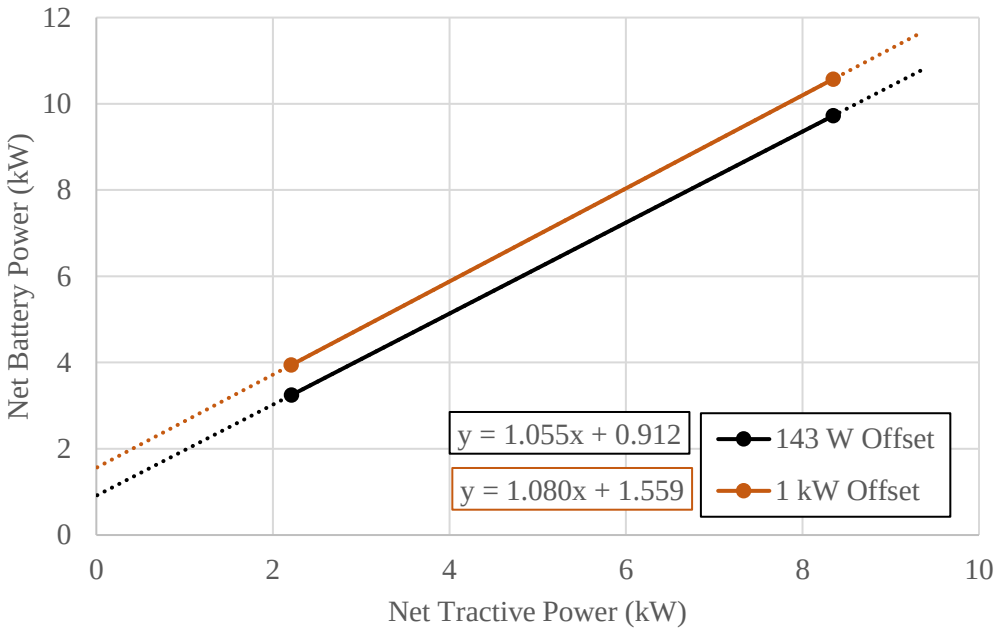

Figure 4.8: *Model Sensitivity to Powertrain Offset*

The third model input parameter studied for model sensitivity is the vehicle accessory load. This input parameter is tuned to be within reasonably expected values for an electric vehicle when tested over the City and Highway cycles. This approach is used due to the vehicle accessory load being an unreported metric in EPA data. Therefore, establishing how sensitive the model is to changes in the vehicle accessory load is of great importance for determining if modeled accessory loads are truly representative of the vehicle. Differentiating Equation 4.3 with respect to only P_{accy} yields the following sensitivity expression

$$\frac{dP_{bat}^{net}}{dP_{accy}} = 1 \tag{4.7}$$

where a direct relationship between changes in vehicle accessory load to cycle average net battery power is observed. As such, each incremental change of vehicle accessory load will subsequently change the cycle average net battery power for both the City and Highway cycles. This relationship is to be expected as the vehicle accessory load is always assumed on, regardless of if the vehicle is in a propel, brake, or idle phase. Table 4.14 contains cycle average net battery power determined from subsequent changes in the vehicle accessory load for the 2017 BMW i3. Reasonable vehicle accessory loads are taken to be between 300 – 850 W as manufacturers are highly conscientious of this power draw to ensure vehicle range is not severely impacted. Therefore, ranges of 0 W to 1.5 kW are chosen as the upper and lower extrema for electric vehicle accessory load as shown in Table 4.14. The subsequent increase or decrease of vehicle accessory load corresponds to an equivalent change in the cycle average net battery power. Figure 4.9 illustrates how the net Willans line changes for corresponding changes in vehicle accessory load. As governed by Equation 4.7, $offset_{net}$ changes linearly with changes in accessory load. At an accessory load of 0 W the presence of a net offset remains as the net Willans line encapsulates regen braking characteristics and the powertrain offset. From Table 4.14 and Figure 4.9 the model is considered moderately sensitive to changes in vehicle accessory load. Because accessory load is not reported by EPA and the major constraining method is by applying reasonable assumptions, determining representative values of accessory load is challenging. Further research would be needed to determine an average electric vehicle accessory load for varying categories of electric vehicles. The proposed modeling method could then leverage this compiled data to provide more accurate results. However, with this sensitivity considered, the proposed modeling method is still considered reasonably accurate for two reasons. The first reason is the vehicle accessory load

affects both the City and Highway cycles equally; therefore, the accessory load is used primarily as a final fitting method for the model. Lastly, the continuous power draw of a vehicle will remain relatively low. Even with peak power considered, the continuous accessory load demand on a vehicle remains relatively constant over a drive cycle. As such, using reasonable assumptions to constrain the ranges of vehicle accessory load still can serve well for tuning the model. With this reasoning in mind, one of the advantages to the proposed method is the ability to study the effects of increased accessory loads due to heating or cooling the vehicle. Altering the vehicle accessory load to account for air conditioning, heating, and other power drawing features of the vehicle can be studied with the proposed method.

Table 4.14: *2017 BMW i3 Sensitivity to Changes in Accessory Load*

Accessory Load	City		Highway	
	Power Change	Net Battery Power	Power Change	Net Battery Power
[W]	[W]	[kW]	[W]	[kW]
0	-315	2.93	-315	9.41
315	0	3.24	0	9.72
1500	1185	4.43	1185	10.9

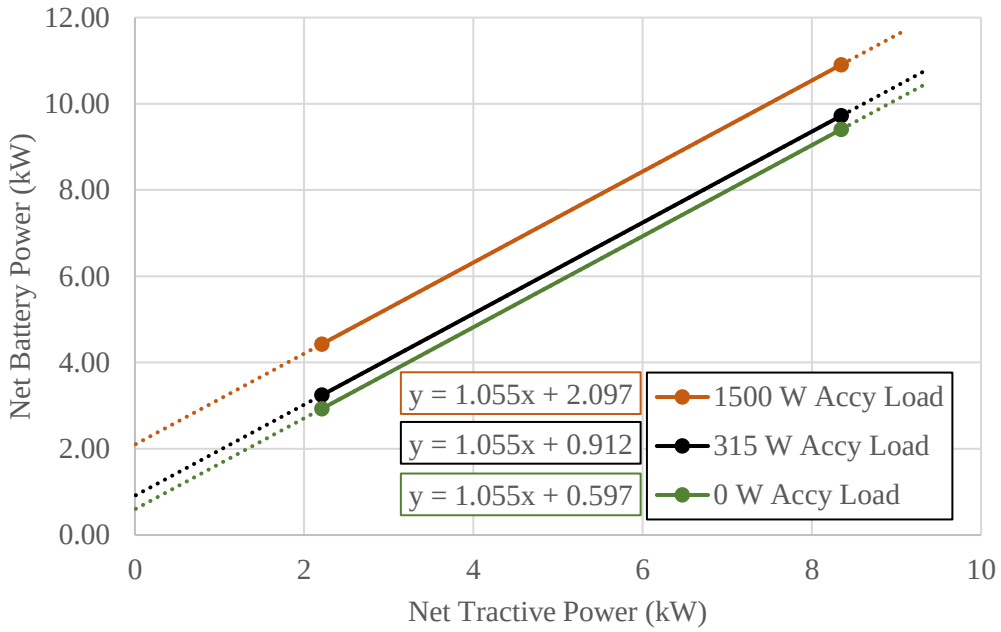

Figure 4.9: *Model Sensitivity to Vehicle Accessory Load*

The regen fraction is additionally studied for model sensitivity as EPA test data does not report an equivalent vehicle regen fraction. Although there is great research and literature on regenerative braking and the limits, the regen fraction is still a major model input for which sensitivity needs to be determined. Taking the derivative of Equation 4.3 with respect to only *RF* yields the final sensitivity expression for the model

$$\frac{dP_{bat}^{net}}{dRF} = \alpha \cdot P_{TR}^{-} \cdot slope^{-} \tag{4.8}$$

where a linear relationship between changes in regen fraction and cycle average net battery power is found. As electric vehicles are built with more powerful motors and proportionally sized batteries, the regenerative capabilities of the vehicle increase. With the powertrain capable of withstanding higher regenerative braking power and current, the regenerative braking limitations for a vehicle would be imposed from a physics and drivability perspective. Some proportion of braking must be supplied by brakes to properly balance the braking of the vehicle. Therefore,

reasonable ranges for regenerative braking fractions are taken to be 75% to 95%. Figures 4.10 and 4.11 illustrate the change in cycle average net battery power for corresponding changes in the set regen fraction. To be expected, the City drive cycle is most sensitive to changes in the regen fraction as this drive cycle has the most braking events when compared to the Highway cycle. Therefore, increasing or decreasing the regen fraction will correspond to less or more of that braking power being recaptured by the motor system. Referring to Table 4.15, reasonable values of the regen fraction are tabulated with the corresponding changes in cycle average net battery. Figure 4.12 illustrates how the net Willans line changes with corresponding changes of the regen fraction. Figure 4.12 illustrates the resiliency of the model to changes in regen fraction as all three curves collapse on one another. To provide additional insight, the City operating point is enlarged to show the deviation between the three curves. When considering a reasonable regen fraction range of 75% to 95%, the model sensitivity is reasonably small. However, including regenerative braking characteristics is still important for developing a bi-directional approach as well as more effectively modeling the vehicle. The reason the model is so resilient to changes in the regen fraction is because the delivered power to the battery during regenerative braking is relatively small compared to what is required for propelling the vehicle. What this assertion means is, changes in regen fraction will not impact the model drastically because a change in regen fraction simply further limits an already limited power source. As such, changes in regen fraction do not impact establishing values for marginal efficiency and offset. To note, similar to the marginal efficiency sensitivity expression, vehicles expend varying P_{TR}^{-} and P_{TR}^{+} over the City and Highway drive cycles. The results presented here are specific to the 2017 BMW i3 which is a light weight, lower capacity, and lower range electric vehicle compared to others. Therefore, greater values of net tractive effort will vary how a specific vehicle changes to tuning of the regen fraction,

and even the marginal efficiency. However despite this fact, the general trends presented in the Sensitivity Analysis section illustrates the powerful resiliency of the model. By applying a bi-directional Willans line from EPA test data, the simplified model illustrates impressive resiliency for a method with four major input parameters. Overall, the results contained within this section illustrate the robustness of the proposed modeling method and yield high confidence for applying the model to determine vehicle energy consumption and powertrain parameters.

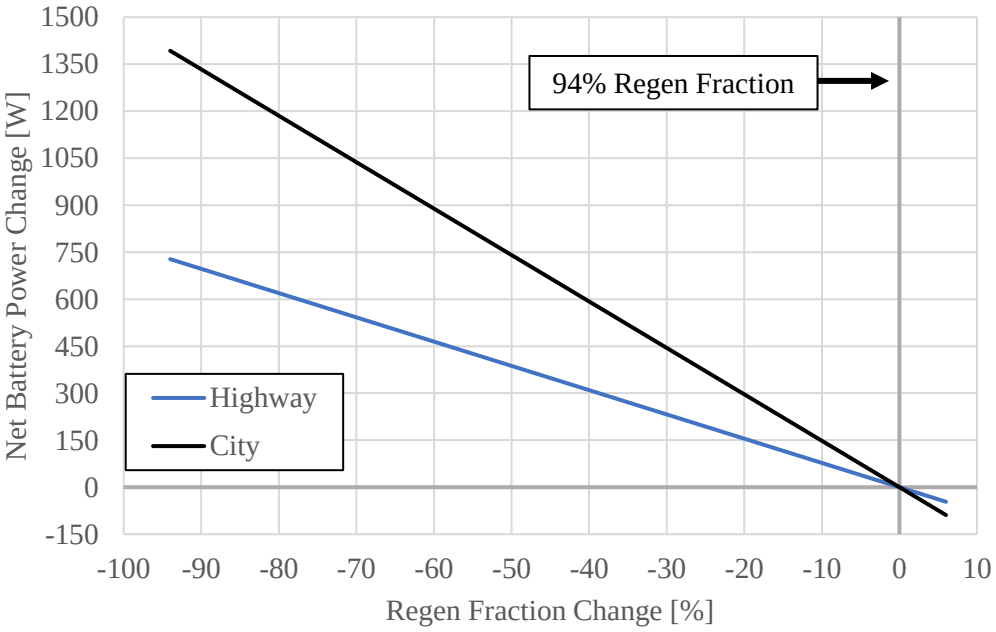

Figure 4.10: *Net Battery Power Change for Finite Changes in Regen Fraction*

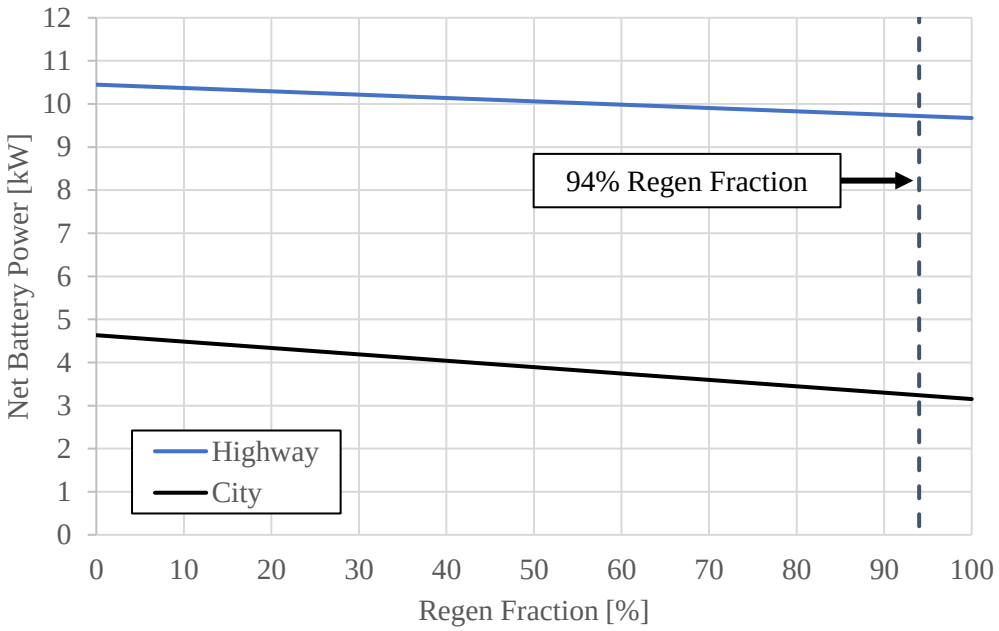

Figure 4.11: *New Cycle Average Net Battery Power for Specific Regen Fractions*

Table 4.15: *2017 BMW i3 Sensitivity to Changes in Regen Fraction*

Regen Fraction	City		Highway	
	Power Change	Net Battery Power	Power Change	Net Battery Power
	[W]	[kW]	[W]	[kW]
75%	282	3.52	147	9.87
80%	207	3.45	108	9.83
85%	133	3.37	69.7	9.79
90%	59.3	3.30	31.0	9.75
94%	0	3.24	0	9.72
100%	-88.9	3.15	-46.5	9.67

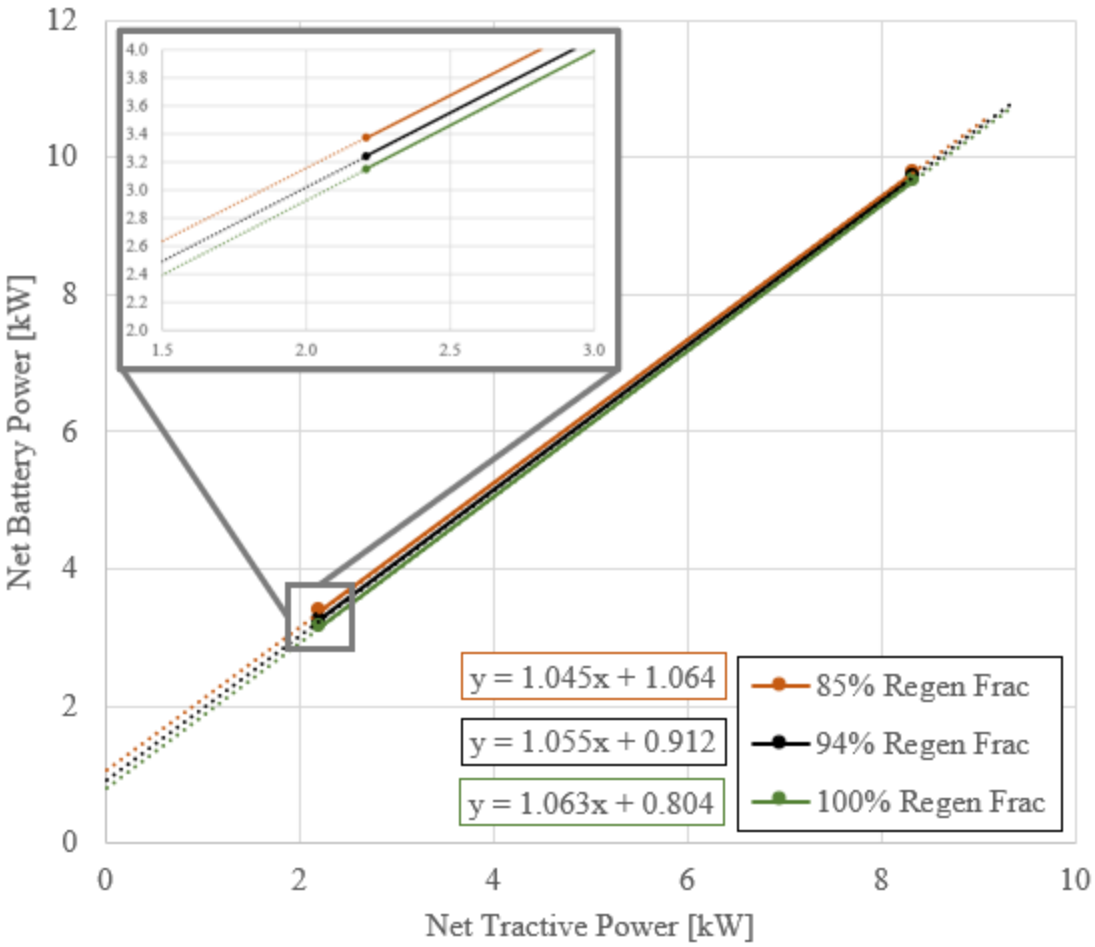

Figure 4.12: *Model Sensitivity to Vehicle Regen Fraction*

Chapter 5
Conclusions

This paper proposes a novel modeling method for estimating electric vehicle powertrain parameters, vehicle net energy consumption, and powertrain efficiency. The first contribution of this work is the development of a bi-directional Willans line for the partitioning of propel and brake phases of electric vehicles. The creation of a bi-directional Willans line better encompasses the battery discharge energy necessary for meeting drive cycle demand. This bi-directional approach also encapsulates the regenerative braking characteristics of the vehicle and establishes how much energy the vehicle recuperates over a drive cycle. The second contribution of this paper is the derivation of a net Willans line intended for proper model input tuning. The method of matching EPA net energy consumption test data by establishing values of powertrain marginal efficiency, offset, vehicle accessory load, and regen fraction is shown to be effective. Utilizing a 2 point method allows for quick and easy establishment of the powertrain parameters and yields reasonable results when the same parameters are used to extrapolate the cycle average net battery power for more aggressive drive cycles. The use of a 3 point method is also investigated with generated results reflecting a minimal change in the powertrain marginal efficiency and offset as established from the 2 point method. Comparing model results to Tesla test data for the US06 City and Highway drive cycles shows percent differences of 1.4% and 3.8% respectively. A derived transfer function between the model inputs and output allows for the sensitivity of the proposed method to be evaluated. The model is deemed effectively resilient to changes in parameters, especially when reasonable ranges for inputs are considered. The model is also shown to be most sensitive to changes in marginal efficiency and accessory load, however most electric vehicles fall

within an expected range for marginal efficiency and the vehicle accessory load affects City and Highway consumption equally. As such, an established value for marginal efficiency is taken to be representative of the vehicle powertrain, and accessory load is used as a final tuning parameter to meet net offset. The proposed method additionally provides insight to the impact of the vehicle accessory load on energy consumption. The proposed method also allows for modeling increased accessory loads for heating, cooling, and other power drawing systems on the vehicle. To this end, the work presented here establishes a simple yet powerful modeling method for evaluating electric vehicles through the novel bi-directional Willans line. The bi-directional Willans line approach is the major contribution with the presented results meeting the objectives of this work.

References

1. E. A. Grunditz and T. Thiringer, “Performance Analysis of Current BEVs Based on a Comprehensive Review of Specifications,” *IEEE Transactions on Transportation Electrification*, vol. 2, no. 3, pp. 270–289, Sep. 2016.

2. A. Fotouhi, K. Propp, S. Longo, and D. J. Auger, “Simulation for prediction of vehicle efficiency, performance, range and lifetime: A review of current techniques and their applicability to current and future testing standards,” *5th IET Hybrid and Electric Vehicles Conference (HEVC 2014)*, Nov. 2014.

3. J. Thomas, “Drive Cycle Powertrain Efficiencies and Trends Derived from EPA Vehicle Dynamometer Results,” *SAE International Journal of Passenger Cars - Mechanical Systems*, vol. 7, no. 4, pp. 1374–1384, 2014.

4. Brooker, A., Gonder, J., Wang, L., Wood, E. et al., "FASTSim: A Model to Estimate Vehicle Efficiency, Cost and Performance," SAE Technical Paper 2015-01-0973, 2015, doi:10.4271/2015-01-0973.

5. Holden, J., Reinicke, N. and Cappellucci, J., “RouteE: A Vehicle Energy Consumption Prediction Engine,” SAE Technical Paper 2020-01-0939, 2020, doi:10.4271/2020-01-0939.

6. Sorrentino, M., Mauramati, F., Arsie, I., Cricchio, A. et al., "Application of Willans Line Method for Internal Combustion Engines Scalability towards the Design and

Optimization of Eco-Innovation Solutions," SAE Technical Paper 2015-24-2397, 2015, doi:10.4271/2015-24-2397.

7. P. Phlips, W. Ruona, T. Megli, and M. Orpe, “Unified Power-Based Vehicle Fuel Consumption Model Covering a Range of Conditions,” SAE Technical Paper 2020-01-1278, 2020.

8. “Data on Cars used for Testing Fuel Economy,” *EPA*, 03-Mar-2021. [Online]. Available: https://www.epa.gov/compliance-and-fuel-economy-data/data-cars-used-testing-fuel-economy. [Accessed: 04-May-2021].

9. “Dynamometer Drive Schedules,” *EPA*, 19-Mar-2021. [Online]. Available: https://www.epa.gov/vehicle-and-fuel-emissions-testing/dynamometer-drive-schedules. [Accessed: 04-May-2021].

10. “EPA's Transportation and Air Quality Document Index System (DIS),” *EPA*. [Online]. Available: https://iaspub.epa.gov/otaqpub/. [Accessed: 04-May-2021].

11. G. Sovran and D. Blaser, “A Contribution to Understanding Automotive Fuel Economy and Its Limits,” SAE Technical Paper 2003-01-2070, 2003.

12. “The official U.S. government source for fuel economy information.,” *www.fueleconomy.gov - the official government source for fuel economy information*. [Online]. Available: https://www.fueleconomy.gov/. [Accessed: 04-May-2021].

13. “SAE Ground Vehicle Standard J1634_202104.” *Light Duty Vehicle Performance and Economy Measure Committee*, 6 Apr. 2021, doi:10.4271/j1634_202104.

14. E. Rask, D. Santini, and H. Lohse-Busch, “Analysis of Input Power, Energy Availability, and Efficiency during Deceleration for X-EV Vehicles,” *SAE International Journal of Alternative Powertrains*, vol. 2, no. 2, pp. 350–361, 2013.

15. E. Nakamura, M. Soga, A. Sakai, A. Otomo, and T. Kobayashi, “Development of Electronically Controlled Brake System for Hybrid Vehicle,” SAE Technical Paper 2002-01-0300, 2002.

Appendix A

Propel, Brake and Net Willans Lines for Modeled Vehicles

2017 BMW i3

Figure A.1 represents the established bi-directional Willans line for the 2017 BMW i3 and Figure A.2 represents the EPA net Willans line. The bi-directional Willans line clearly uses the set powertrain marginal efficiency and offset to model the instantaneous power flow to go from tractive power to motor power. The EPA net Willans line represents the derived fit for the City and Highway cycles with the net offset and net slope displayed as an equation. The 2017 BMW i3 net energy consumption data provided by EPA is used to match the model net Willans line when the propel and brake events are summed over each drive cycle.

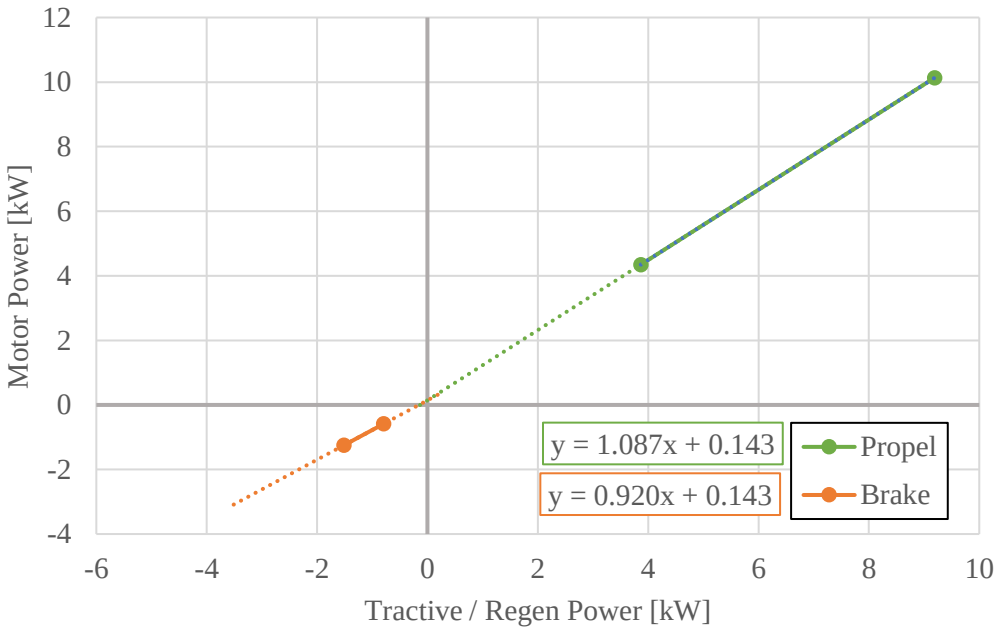

Figure A.1: *2017 BMW i3 Bi-Directional Willans Line*

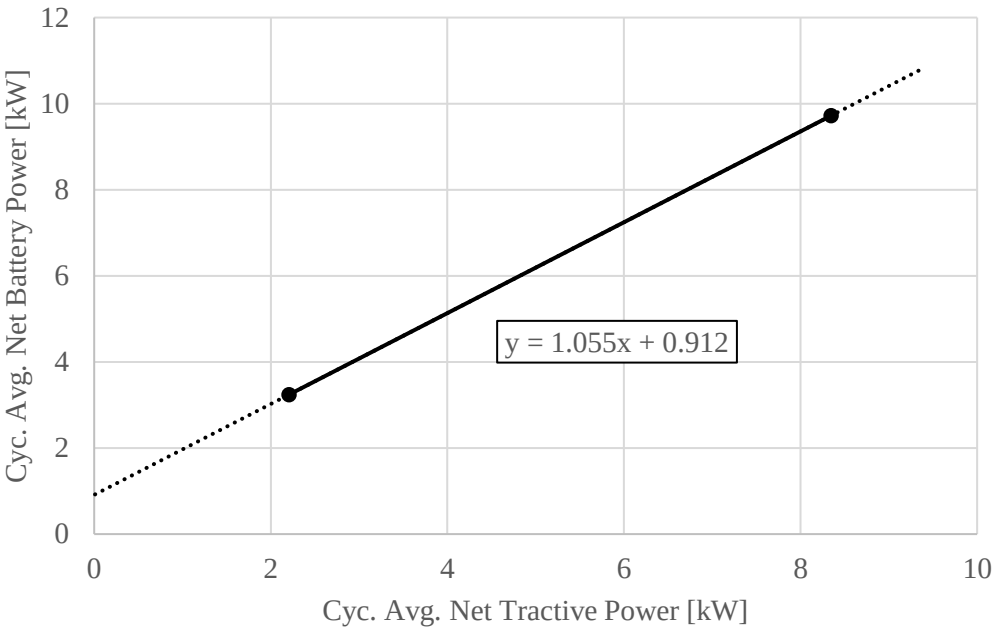

Figure A.2: *2017 BMW i3 EPA Net Willans Line*

2020 Chevrolet Bolt

Figure A.3 represents the established bi-directional Willans line for the 2020 Chevrolet Bolt and Figure A.4 represents the EPA net Willans line. The bi-directional Willans line illustrates the set powertrain parameters for the Chevrolet Bolt as 97.7% for the marginal efficiency and 160 W for the offset. The net Willans line derived from EPA data captures the net slope being less than unity as the Chevrolet Bolt has a derived ME_{net} which is greater than 100%. Therefore, the Chevrolet Bolt is one of the two chosen vehicles with a regen fraction less than 94%.

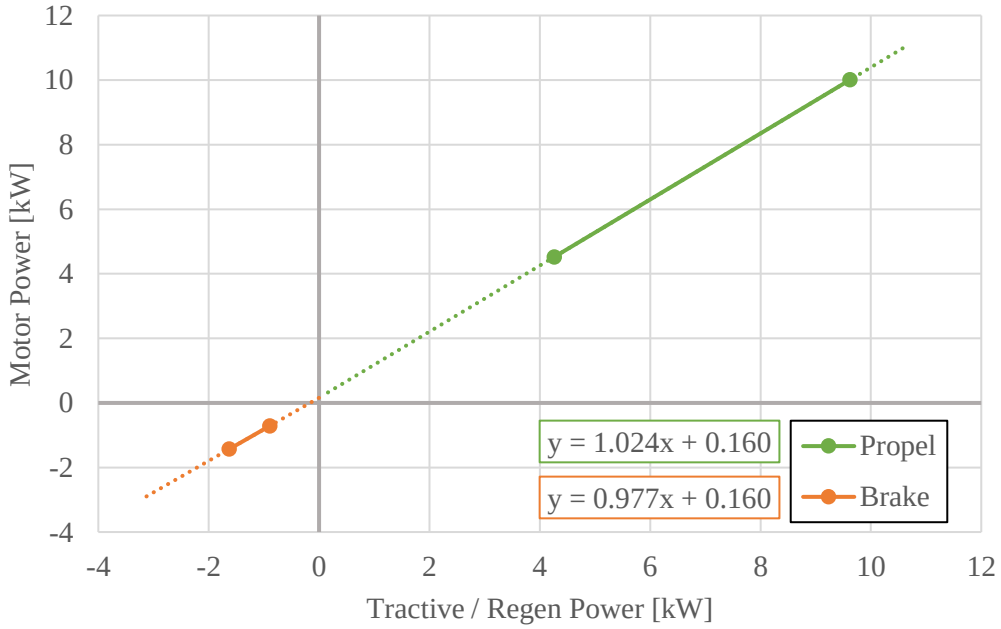

Figure A.3: *2020 Chevrolet Bolt Bi-Directional Willans Line*

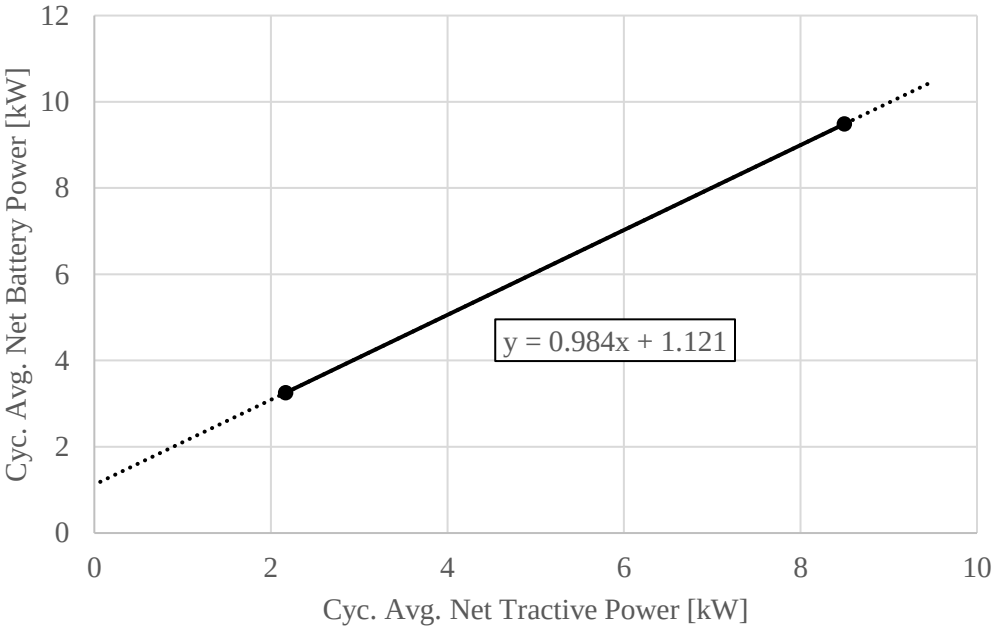

Figure A.4: *2020 Chevrolet Bolt EPA Net Willans Line*

2021 Ford Mustang Mach-E Standard Range

Figure A.5 represents the established bi-directional Willans line for the 2021 Ford Mustang Mach-E Standard Range and Figure A.6 represents the EPA net Willans line. The bi-directional Willans line contains the set powertrain parameters for the Standard Range Mach-E as 94.9% for the marginal efficiency and 650 W for the offset. The net Willans line derived from EPA data was used to tune the bi-directional Willans line to yield a model net Willans line which matches Figure A.6.

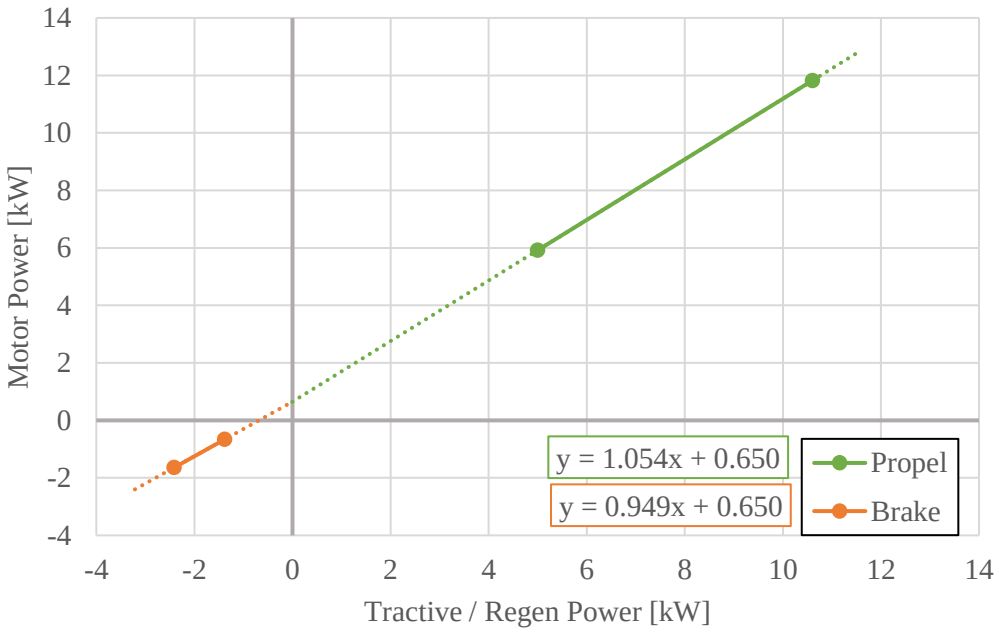

Figure A.5: *2021Mustang Mach-E Standard Range Bi-Directional Willans Line*

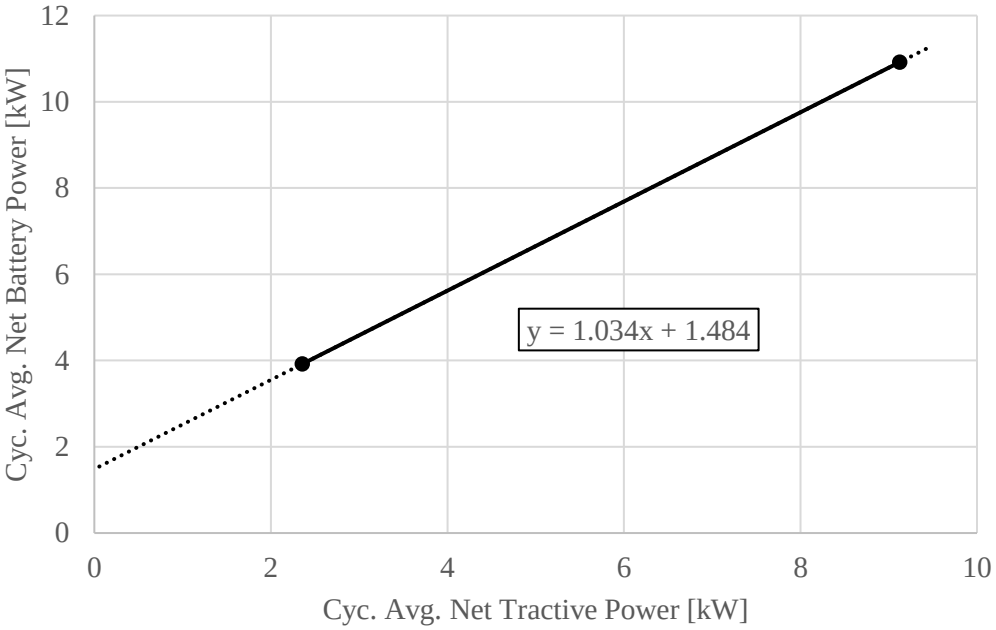

Figure A.6: *2021 Mustang Mach-E Standard Range EPA Net Willans Line*

2021 Ford Mustang Mach-E Extended Range

Figure A.7 represents the established bi-directional Willans line for the 2021 Ford Mustang Mach-E Extended Range and Figure A.8 represents the EPA net Willans line. The bi-directional Willans line contains the set powertrain parameters for the Extended Range Mach-E as 92% for the marginal efficiency and 246 W for the offset. The net Willans line derived from EPA data was used to tune the bi-directional Willans line to yield a model net Willans line which matches Figure A.8.

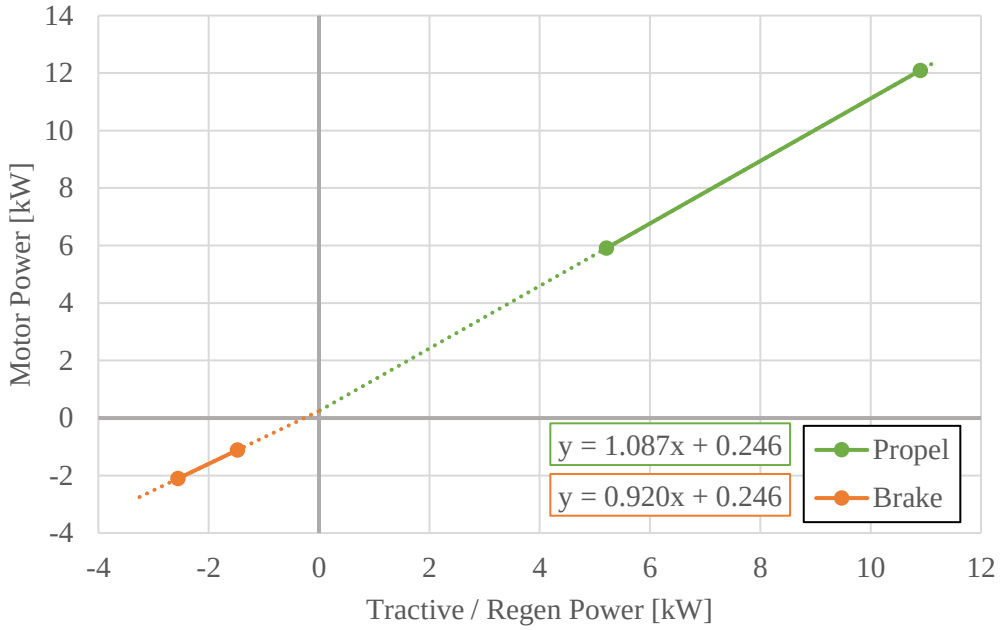

Figure A.7: *2021 Mustang Mach-E Extended Range Bi-Directional Willans Line*

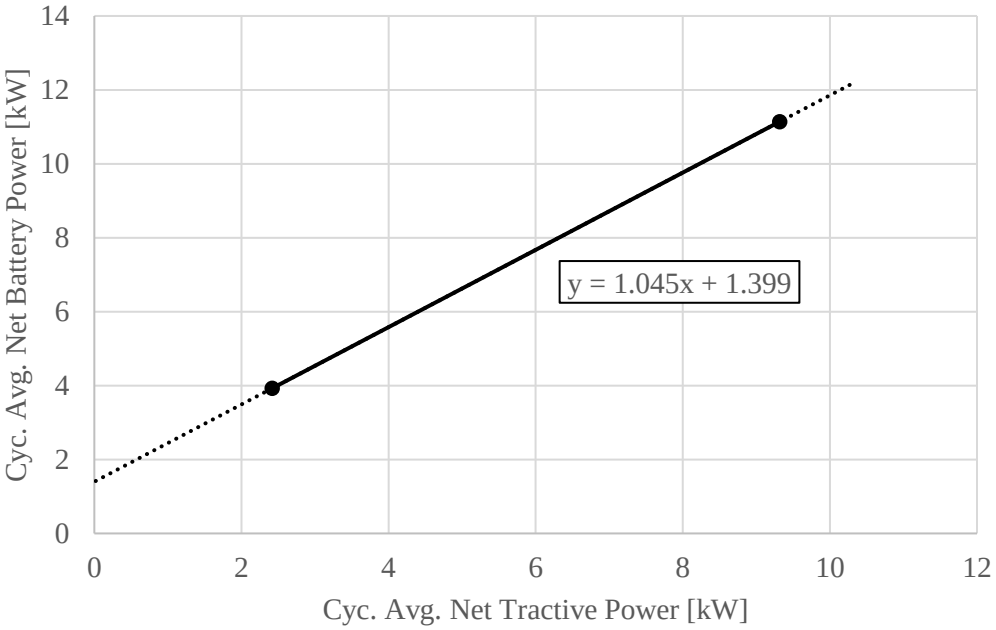

Figure A.8: *2021 Mustang Mach-E Extended Range EPA Net Willans Line*

2019 Jaguar I-Pace

Figure A.9 represents the established bi-directional Willans line for the 2019 Jaguar I-Pace and Figure A.10 represents the EPA net Willans line. The bi-directional Willans line contains the set powertrain parameters for the Jaguar I-Pace as 97.5% for the marginal efficiency and 790 W for the offset. The net Willans line derived from EPA data was used to tune the bi-directional Willans line to yield a model net Willans line which matches Figure A.10.

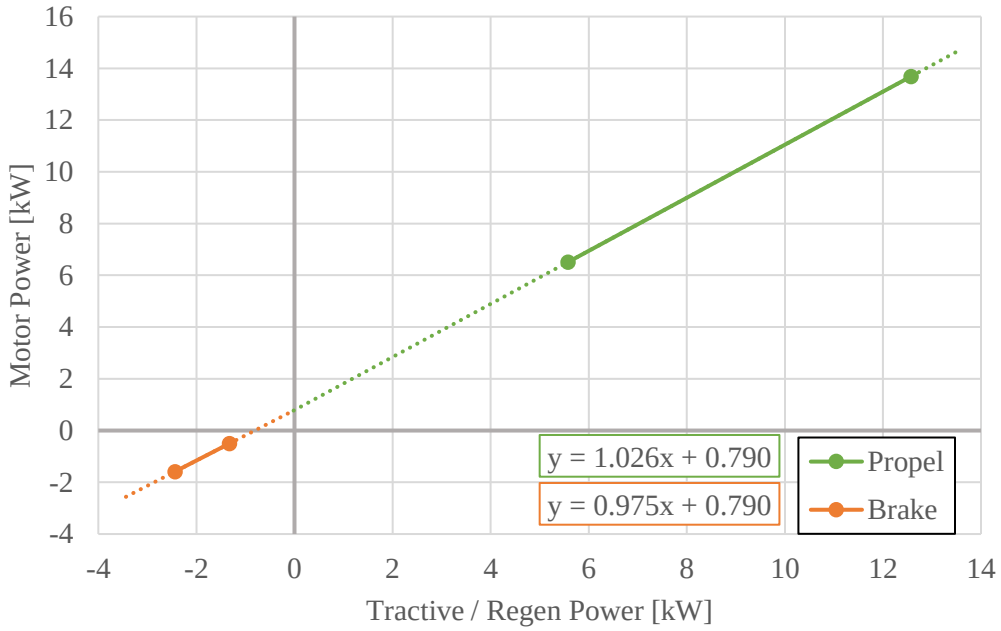

Figure A.9: *2019 Jaguar I-Pace Bi-Directional Willans Line*

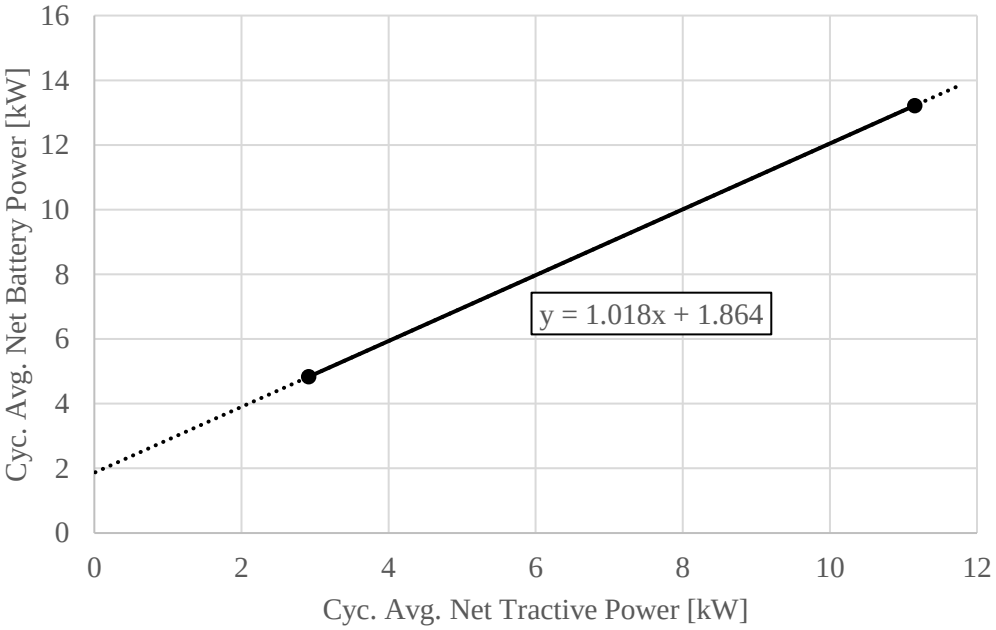

Figure A.10: *2019 Jaguar I-Pace EPA Net Willans Line*

2016 Nissan Leaf

Figure A.11 represents the established bi-directional Willans line for the 2016 Nissan Leaf and Figure A.12 represents the EPA net Willans line. The bi-directional Willans line contains the set powertrain parameters for the Nissan Leaf as 97% for the marginal efficiency and 184 W for the offset. The net Willans line derived from EPA data was used to tune the bi-directional Willans line to yield a model net Willans line which matches Figure A.12.

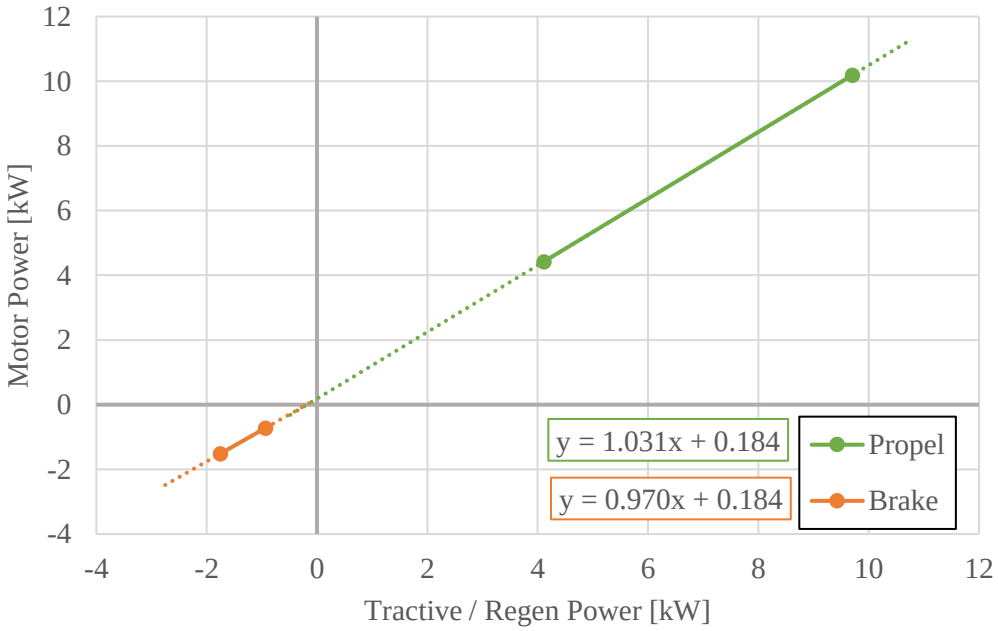

Figure A.11: *2016 Nissan Leaf Bi-Directional Willans Line*

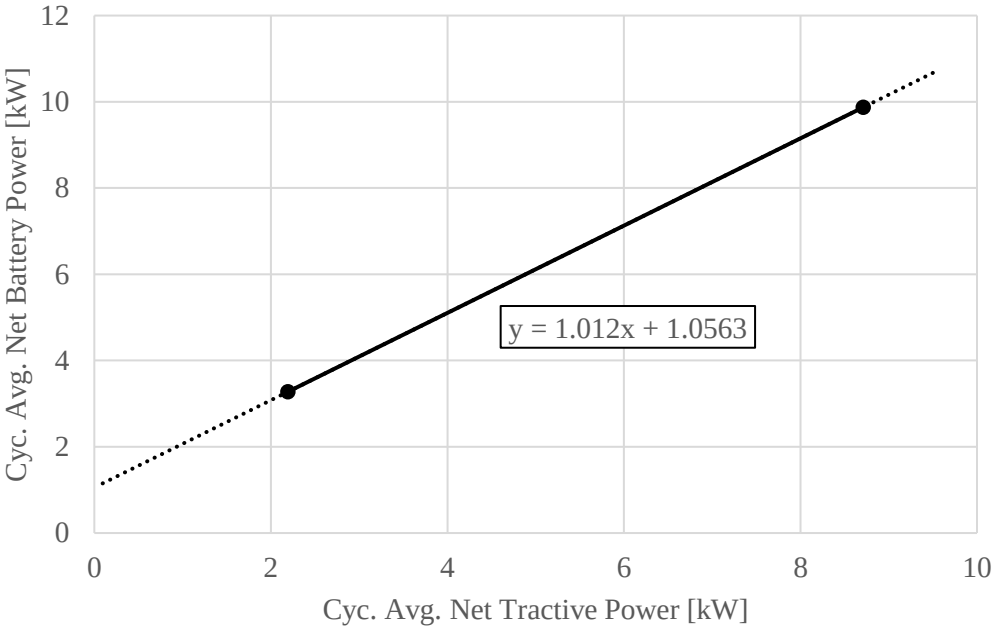

Figure A.12: *2016 Nissan Leaf EPA Net Willans Line*

2020 Porsche Taycan Turbo

Figure A.13 represents the established bi-directional Willans line for the 2020 Porsche Taycan Turbo and Figure A.14 represents the EPA net Willans line. The bi-directional Willans line contains the set powertrain parameters for the Taycan Turbo as 89% for the marginal efficiency and 900 W for the offset. The net Willans line derived from EPA data was used to tune the bi-directional Willans line to yield a model net Willans line which matches Figure A.14.

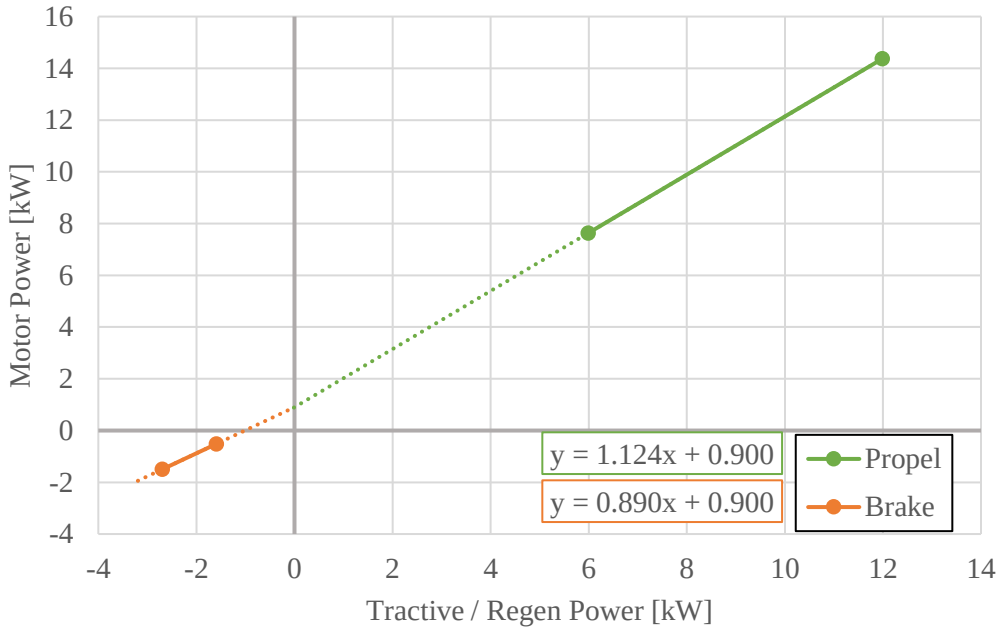

Figure A.13: *2020 Porsche Taycan Turbo Bi-Directional Willans Line*

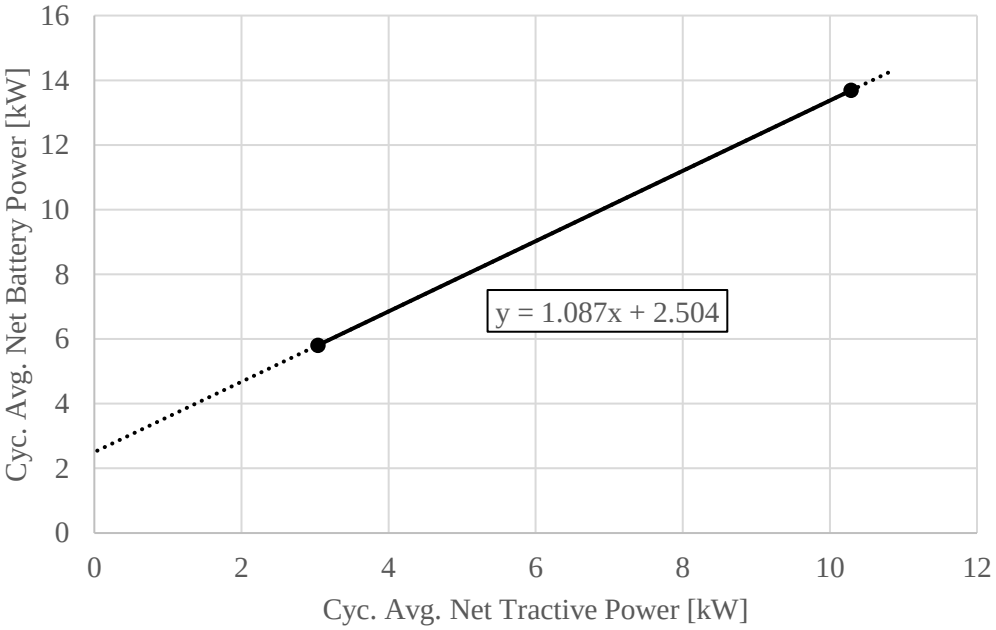

Figure A.14: *2020 Porsche Taycan Turbo EPA Net Willans Line*

2019 Tesla Model X Long Range

Figure A.15 represents the established bi-directional Willans line for the 2019 Tesla Model X Long Range and Figure A.16 represents the EPA net Willans line. The bi-directional Willans line contains the set powertrain parameters for the Model X Long Range as 98.3% for the marginal efficiency and 173 W for the offset. The net Willans line derived from EPA data was used to tune the bi-directional Willans line to yield a model net Willans line which matches Figure A.16.

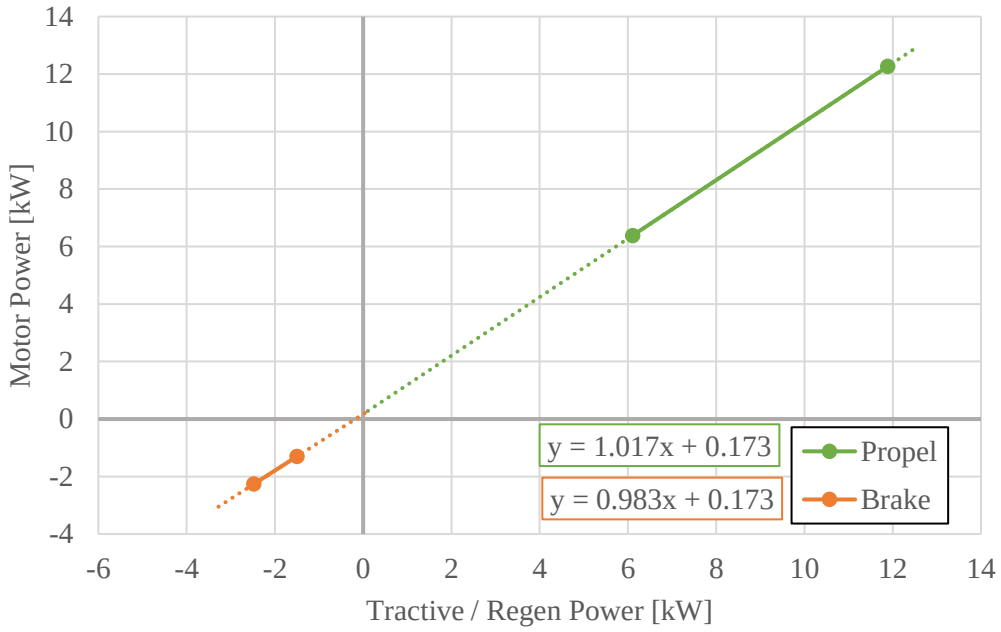

Figure A.15: *2019 Tesla Model X Long Range Bi-Directional Willans Line*

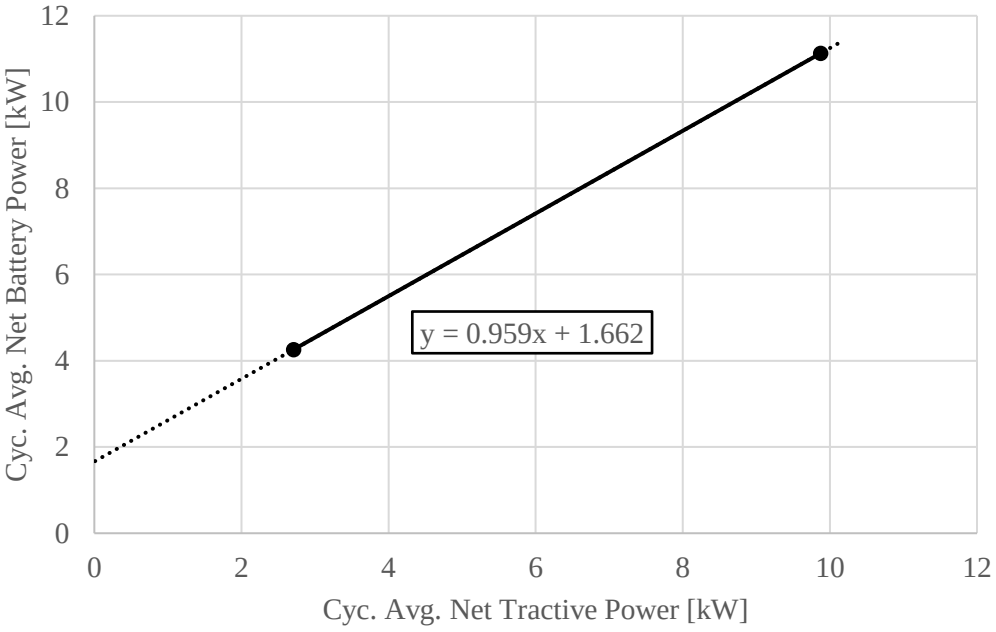

Figure A.16: *2019 Tesla Model X Long Range EPA Net Willans Line*